NTNU
Det skapende universitet

Utmattingslevetiden av limfuger

Erik Sæter

Master i produktutvikling og produksjon
Innlevert: juni 2016
Hovedveileder: Andreas Echtermeyer, IPM

Norges teknisk-naturvitenskapelige universitet
Institutt for produktutvikling og materialer

Problem text

NTNU - NORWEGIAN UNIVERSITY
OF SCIENCE AND TECHNOLOGY
DEPARTMENT OF ENGINEERING DESIGN
AND MATERIALS

MASTER THESIS SPRING 2016
FOR
STUD.TECHN. ERIK SÆTER

Fatigue resistance of adhesive joints

Utmattingslevetiden av limfuger

This project investigates composite metal joints. Examples of applications are offshore structures, ships, trucks and bridges.

The project will investigate resistance to fatigue loading by measuring and analyzing damage initiation, propagation and final failure. Joints shall be analyzed by finite element analysis and they shall be tested experimentally. Strain fields and their changes will be measured with optical fibers and strain gauges.
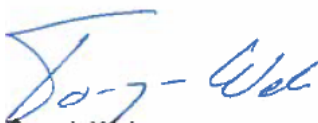
Formal requirements:

Three weeks after start of the thesis work, an A3 sheet illustrating the work is to be handed in. A template for this presentation is available on the IPM's web site under the menu "Masteroppgave" (https://www.ntnu.edu/web/ipm/master-thesis). This sheet should be updated one week before the master's thesis is submitted.

Risk assessment of experimental activities shall always be performed. Experimental work defined in the problem description shall be planed and risk assessed up-front and within 3 weeks after receiving the problem text. Any specific experimental activities which are not properly covered by the general risk assessment shall be particularly assessed before performing the experimental work. Risk assessments should be signed by the supervisor and copies shall be included in the appendix of the thesis.

The thesis should include the signed problem text, and be written as a research report with summary both in English and Norwegian, conclusion, literature references, table of contents, etc. During preparation of the text, the candidate should make efforts to create a well arranged and well written report. To ease the evaluation of the thesis, it is important to cross-reference text, tables and figures. For evaluation of the work a thorough discussion of results is appreciated.

The thesis shall be submitted electronically via DAIM, NTNU's system for Digital Archiving and Submission of Master's theses.

Torgeir Welo
Head of Division

Andreas Echtermeyer
Professor/Supervisor

NTNU
Norges teknisk-
naturvitenskapelige universitet
Institutt for produktutvikling
og materialer

i

Preface

This thesis is written in the spring of 2016 at the Department of Engineering and Materials at NTNU. The work is a continuation of the pre master project carried out in the fall of 2015. My interest in the field of composite materials is one of the reasons why I chose this project.

The work has mainly been split between experimental work and strain field analysis. Some time was spent on sample preparation and testing to gather the necessary data. The main focus of the project, particularly in the late stages, has been the strain field analysis. The experimental tests provide a lot of data. Systemization and interpretation is time consuming but has in the end provided interesting results.

The use of FEA was a planned activity, but was not achieved during this project. The time consuming nature of the strain field analysis took too much time away from properly engaging in the work of investigating crack initiation with FEA.

I would like to thank my supervisor Andreas Echtermeyer who has provided me with help, guidance and knowledge throughout the process.

Also thanks to PhD Jon Harald Lambert Grave for his contribution with structural health monitoring by the use of optic fibres, experimental setup and information. I would also like to thank PhD candidate Sören Heinze for guidance in the use of optical fibres, both practical use and introduction to analysis. His self-made programs for recording measurements during testing and writing of .txt files for analyses were invaluable.

Abstract

The use of adhesive joints allows for composite materials to aid in the structure of other materials. Especially during repairs of large structures, this can prove valuable. The long term effect of the use of composite materials in structural repairs is still not fully known.

This thesis has explored the effect of fatigue on single lap joints through experimental work and strain field analysis. The main focus was 100 mm overlap single lap joints with steel and carbon fibre reinforced adherends. There were two configurations of composite materials, high modulus and ultra high modulus carbon fibre. The samples were prepared with optical fibres and strain gauges for health monitoring. SN curves were established both for number of cycles to failure and crack initiation. In addition the optical fibres where used to track and compare crack propagation both on the surface of the sample and in the bond line.

Sammendrag

Bruken av limte forbindelser gjør det mulig å benytte kompositmaterialer til reparasjon av strukturer laget av ulike materialer. Spesielt ved reparasjon av store strukturer kan dette vise seg å være verdifullt. Langtidsegenskapene ved bruken av kompositmaterialer er ennå ikke fullt kjent.

Denne masteroppgaven har undersøkt effekten av utmatting på «single lap»-forbindelser gjennom eksperimentelt arbeid og tøyningsfeltanalyse. Hovedfokus har vært på 100 mm «single lap»-forbindelser bestående av stål og karbonfiber-laminater. Det var to typer konfigurasjoner av kompositmaterialet, «high modulus» og «ultra high modulus». Prøvene ble forberedt med optiske fibre og strekklapper brukt til å overvåke tilstanden til prøvene underveis i testingen. SN-kruver ble etablert ut fra innsamlede resultater både for levetid og initiering av sprekk. I tillegg har de optiske fibrene blitt benyttet til å undersøke og sammenligne sprekkveksten både på overflaten av prøven og i limforbindelsen.

Contents

List of figures

List of tables

List of symbols

F = Load [kN]
A = Area [mm^2]
τ = Shear stress [MPa]
τ_{max} = Max shear stress [MPa]
τ_0 = Shear stress limit for 1 fatigue cycle [MPa]
N = Number of cycles

1 Introduction

The use of composites in the field of materials has increased in the last years. Applications can be found everywhere – from the hobby market to aerospace engineering. Stiffness and strength is often marketed as the trademark of these materials, which in many cases make them optimal for large structures.

In modern society there are still a myriad bridges, buildings and other constructions made by other materials than composites – one reason being that steel and aluminium have been just as good for the task at hand. Another reason could be that the availability of materials at the time of construction limited the use of anything other than metals. However, in both cases the need for repairs could be necessary. Sometimes the use of welding can lead to fire hazards or the working space does not allow for such a method of repair. As a mean to solve this problem, it has been proposed that composite materials could be used to restore the structural integrity of the construction.

While there are examples of composites used for repairs at this time, the use of composite materials is not yet fully utilized. Establishing credibility in the use of composite materials is necessary and extensive testing and documentation will help in that area. This project has investigated the effects of fatigue on an adhesive joint through experimental work by investigating crack initiation, propagation and life. The joint investigated in this work is the single lap joint.

Some parts of this thesis have been adopted from the pre-master project, *Fatigue optimization in metal-composite bonds* [1], carried out in the fall of 2015.

2 Theory

2.1 Single lap joints

Adhesive joints are bonded assemblies consisting of adherends and a substrate, bonded together. The benefits of adhesive joints include, according to Vassilopoulos (2012) [2], a more uniform distribution of stresses compared to riveting or similar, possibility of mixing materials and a high fatigue resistance. Figure 1 shows an illustration of an adhesive joint. This joint in particular is the previously mentioned single lap joint. In this project the two adherends are a steel and a carbon fibre composite laminate.
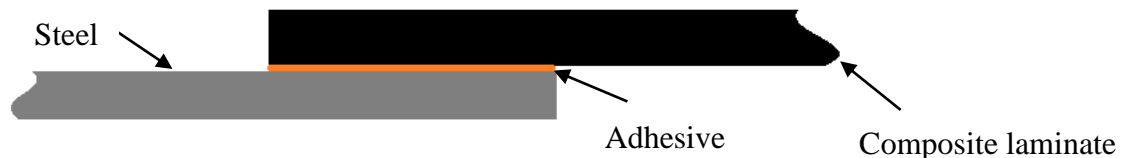
Figure 1: Adhesive joint

In a single lap joint the load is transferred from one adherend, through the adhesive, and trough the other adherend. During tension the adherends will stretch, however the stiffness off the overlap will be greater than the adherends alone. This difference in stiffness leads to an increase in the shear stress in the areas where the overlaps start. As seen in figure 2 the shear stresses are larger in the ends of the overlap. The non-uniformity is often called differential strain. These shear stresses are what leads to the so called bathtub curve, which can be seen in the same figure.
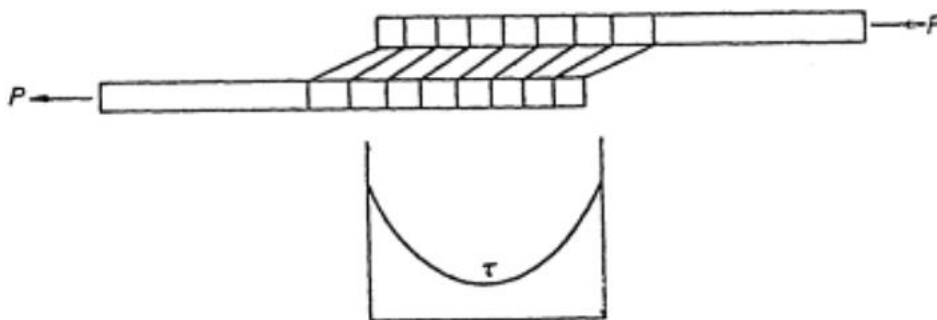
Figure 2: Non-uniform shear distribution in adhesive layer. From [3]

During loading, the joint will deform as shown in Figure 3. The adherends will try to peel from each other resulting in additional stress concentrations in the zones were the overlaps end. This is what is referred to as adhesive peel stresses. With high adhesive strength this can lead to yielding or interlaminar failures in the adherends (depending on the material). An example of interlaminar failure can be seen in Figure 4. The peel stresses, in transverse direction, tears the laminate apart, thereby reducing the ability of shear transfer locally. According to Vassilopoulos (2012) [2], the peel loads are the most critical in single lap joints, especially for composite materials, where they lead to interlaminar failure before adhesive debonding occurs.
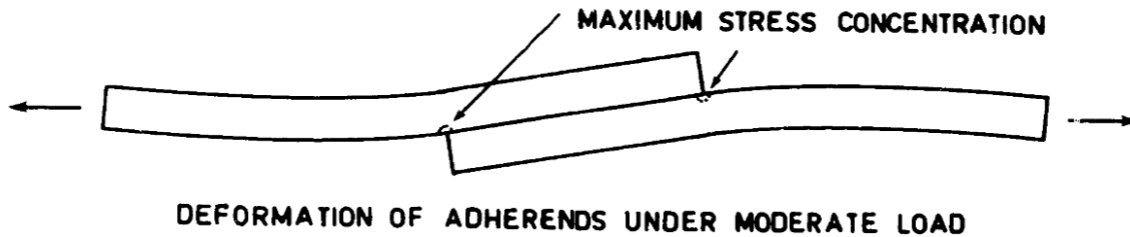
Figure 3: Deformation and stress concentrations in tensioned single lap joints. From [4]
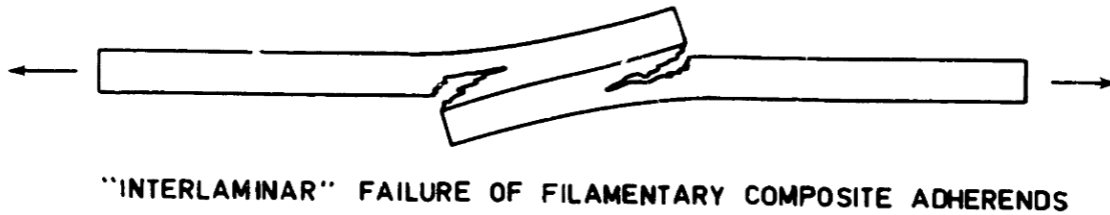
Figure 4: Interlaminar failure in composite-composite single lap joint. From [4]

2.2 Factors affecting joint strength

The factors influencing joint strength are material properties of adhesives and adherends, as well as the geometrical parameters of adhesive and adherends. The geometry parameters include thickness of adhesive, and thickness and area of the overlap.

As seen in section 2.1 the overlap has a non-uniform stress distribution. The middle section sees fairly low stresses, meaning the stress concentrated areas are where failure occurs. The work of improving the strength of the joint is therefore focused on reducing the stress concentrations. Guidelines for this are given by Vassilopoulos (2012) [2]:

- The use of an adhesive with low modulus and ductile behaviour
- Use adherends with similar stiffness, usually from the use of similar adherends.
- The use of a thin adhesive layer.
- Ensure a large bonded area.

A more thorough description of each point follows.

2.2.1 Adhesive properties

The strength of an adhesive is usually not the best indicator of the strength of a joint. While the adhesive need to have adequate strength to handle the shear load, a strong adhesive will in most cases have a high stiffness and a low ductility. These two parameters will decrease the ability of distributing stresses uniformly in the overlap. See Figure 5 for a comparison between stiff and flexible adhesives. As seen in the figure, the stress concentrations are lower for the low stiffness adhesive joint. The plastic deformation which can occur in adhesive materials with lower strength will also be beneficial when it comes to making the joint stronger compared to adhesives that, on their own, are stronger but less ductile. The ductility makes an adhesive able to redistribute the loads so that a larger part of the adhesive surface

can be used to support the shear. An adhesive with low ductility will not be able to redistribute the loads and will therefore have a lower average shear stress (Figure 6).

Although the properties of the adhesive; strength, ductility and stiffness are independent, it is very difficult to create a material with high strength, high ductility and low stiffness. The compromise of going with a lower strength adhesive (with low stiffness and high ductility) is therefore recommended.

When fatigue is considered there is also a benefit having a ductile material. Their resistance to crack propagation as a result of the ductility is one reason, another one being the higher damping energy.
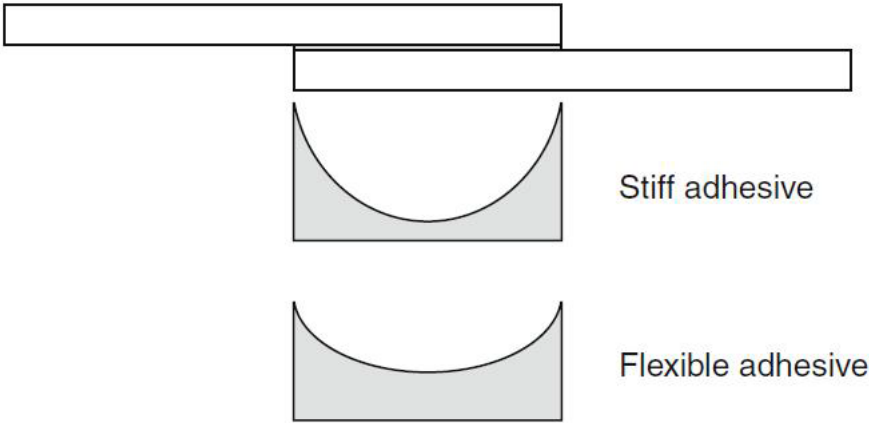
Figure 5: Effect of adhesive stiffness on adhesive stress distribution. From [2]
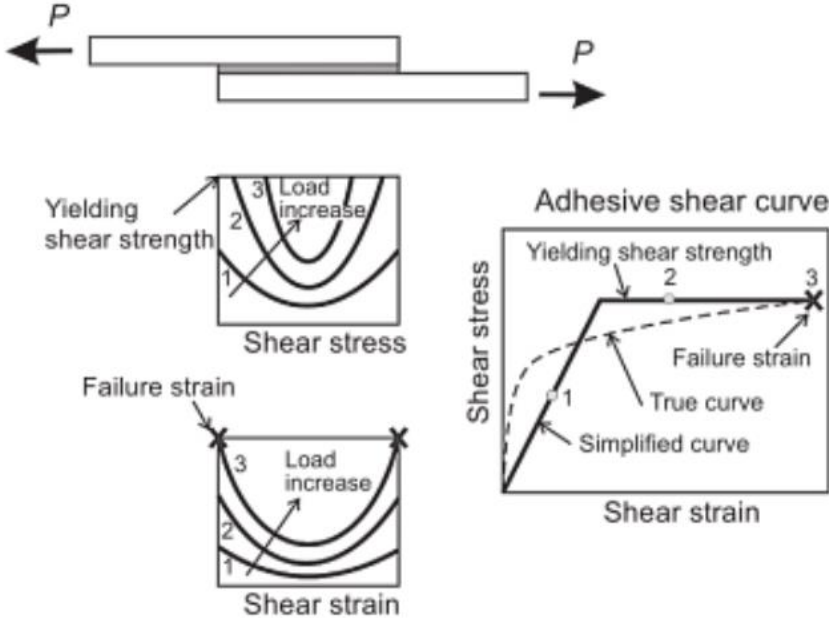
Figure 6: The effect of adhesive ductillity on stress distribution. From [2]

Campilho (2015) [7] mentions a way of improving the adhesive bond by utilizing more than one adhesive. A brittle adhesive is used in the center area of the overlap and a ductile adhesive is used in the higher stress overlap end areas. When the load carried by the brittle

4

adhesive area is higher than that of the ductile adhesive, the total strength of the joint will be higher than that of a joint comprised only of a brittle adhesive.

2.2.2 Adherend properties

As seen in Figure 2, the strain of the adherends when entering the overlap lead to the non-uniform stress distribution. A stiff adherend will deform less, meaning lower differential strain [2].

The strength is also of importance. When the loads increase the stresses increase in the ends of the overlaps (figure 3) and when they turn sufficiently large the adherends can yield, in the case of a metal. For the samples in this thesis the strength of the steel will be much greater than that of the composite, which means that failure of the steel is highly unlikely. The composite on the other hand will have to be taken into consideration. Having fibres in the axial direction is necessary to counter the membrane stresses from compression. Transverse fibres, in the direction of width, could suffer interlaminar failure [2]. The main concern is however the previously mentioned peel stress. The low transverse strength through the thickness of the laminate cannot be higher than the adhesive tensile strength. The damage progression of this issue can be seen in Figure 7.
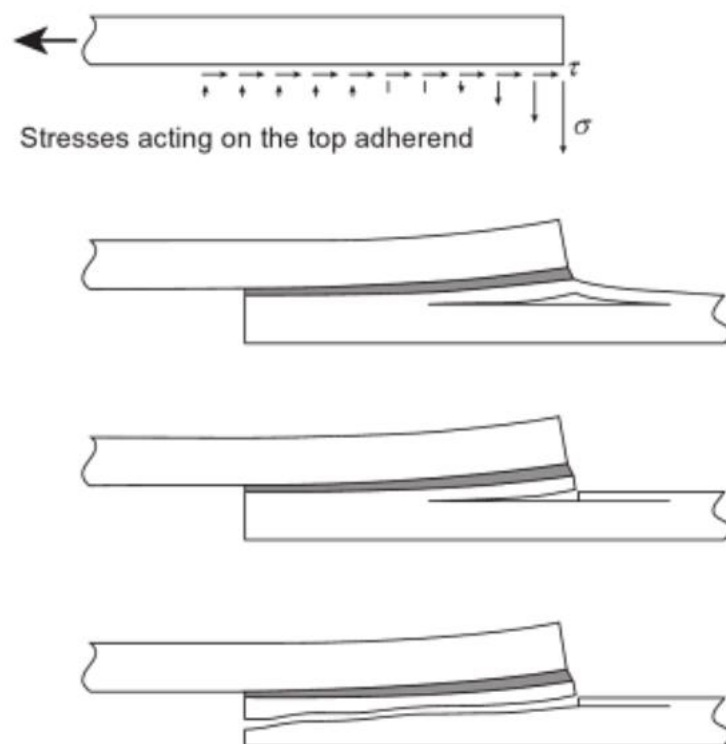
Figure 7: Development of interlaminar failure in composite adherend. From [2]

Other adherend concerns worth mentioning is the use of adherends with differing stiffnesses. This will also lead to a non uniform distribution of stresses, where the concentration peaks will be higher on the low stiffness side. In practical applications, for instance where composite patches will be used for repairs, this is an issue that has to be taken into consideration. A practical solution to altering the stiffness is considering the thickness of the adherends. By reducing the thickness of the adherend towards the end of the laminate, known as tapering, the peel stress will be reduced [2].

2.2.3 Thickness of adhesive

Experimentally it has been proven for metal joints that an adhesive bond in the range of 0.1 to 0.2 mm is beneficial. Analytical models on the other hand often seem to contradict the experimental work. For composites in a single lap joint *a decrease in the adhesive stiffness increases the peel stress at the end of the overlap and might trigger composite delamination* [2]. This is given as an argument saying that there might be a reduced effect of a thin bond line.

2.2.4 Overlap area

For a given overlap length, increasing the width will give a proportional increase in strength.

3 Experimental work

The experimental work done is a continuation of the work done in the pre-master project in the fall of 2015. A total of 8 specimens with an overlap length of 100 mm were to be analysed. Six were already tested, but two remained for experimental work in the thesis. In addition two samples with an overlap of 200 mm were prepared and tested.

Prior to testing the samples had to be prepared by installing strain gauges and preparing the optical fibre. The optical fibre inside the laminate has to be spliced to an optical fibre used to measure strain on the top side of the composite adherend.

3.1 Sample information

All the samples tested were prefabricated by John Harald Lambert Grave. The samples were made according to specifications of the Co-patch project [6] indicated in figure 8 and figure 9.
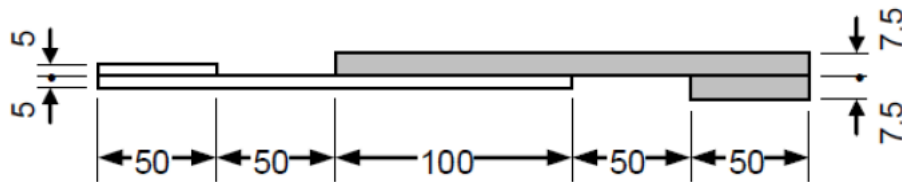
Figure 8: Geometry of 100 mm overlap specimens, units in mm. From [6]
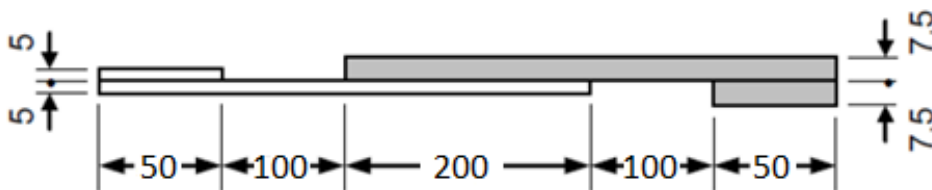
Figure 9: Geometry of 200 mm overlap specimens, units in mm. From [6]

There were two types of single lap joints tested. Both types had the same steel adherend, but one type had a high modulus carbon (HMC) fibre adherend and the other had an ultra high modulus carbon (UHMC) fibre adherend. In order to measure the strain in the bond the optical fibre is embedded in the laminate. The different types can be broken down in the following overview of the lay-up configuration:

HMC samples: Steel + SA80 + PP + Optical fibre + HMC
UHMC samples: Steel + SA80 +PP + Optical fibre + UHMC

The composite materials used were from Gurit. They are high modulus and ultra high modulus carbon fibre composites respectively with the resin system SE84LV. The PP is a pre-preg material consisting of a glass fibre, RE295, with the resin system SE84LV. It is used for electrical isolation to prevent galvanic corrosion. The SA80 is an adhesive film used in conjunction with the SE84LV pre-pregs to increase the bond strength. As seen from the configuration the optic fibre is positioned directly under the carbon composite laminate. This means it is able to measure the strains in the adhesive.

For keeping track of the samples, they were all marked and given their specific number. Table 1 shows the identification of the samples. Fibre optic data and data files from Catman are designated with the prefix SLJ_ in addition to the sample name. These are all the samples analysed in this thesis.

Specimen name	Optic fibre and Catman file name
HMC100_1	SLJ_HMC100_1
HMC100_2	SLJ_HMC100_2
HMC100_3	SLJ_HMC100_3
HMC100_4	SLJ_HMC100_4
UHMC100_1	SLJ_UHMC100_1
UHMC100_2	SLJ_UHMC100_2
UHMC100_3	SLJ_UHMC100_3
UHMC100_4	SLJ_UHMC100_4

Table 1: Specimen overview 100 mm overlap

In addition the 200 mm samples tested are summarized in table 2:

Specimen name	Optic fibre and Catman file name
HMC200_5	SLJ_HMC200_5
UHMC200_1	SLJ_UHMC200_1

Table 2 Specimen overiew 200 mm overlap

3.2 Preparing samples for testing

3.2.1 General preparation

When the samples were collected from storage it was obvious that the water jet had not done the job properly. As seen in the Figure 9, several samples were not fully cut through. In order to fix these samples a bandsaw was used. The job was fairly simple when the stuck sections were close to the outer edge but care still had to be taken to avoid damage to the embedded optical fibre. When the samples were separated it was time to record the geometrical data.

Figure 10: Water jet not fully cut through the laminate.

In order to gather as much information as possible from testing and as an important role in determining the shear strength of the bond it was important to measure and document all the samples thoroughly. Samples were measured in the following procedure:

- Width: Take several measurements alongside the overlap in order to determine the average width. 5 measurements were taken, equally spaced along the overlap section.
- Overlap length: Measure both sides of the overlap to determine average length of the overlap.

From the above procedure the area of the bond can be calculated. The results are summarized in Table 3 below. Table 11 in the appendix A.1 shows all the raw data.

Specimen	Average width [mm]	Average length [mm]	Overlap area [mm²]
HMC 100_1	25,06	98,95	2479,7
HMC 100_2	25,00	98,85	2471,3
HMC 100_3	24,46	98,4	2406,9
HMC 100_4	23,38	98,15	2294,7
UHMC 100_1	25,28	99,4	2512,8
UHMC 100_2	23,7	99,25	2352,2
UHMC 100_3	30,00	99,1	2973
UHMC100_4	24,94	99,05	2470,3
HMC200_5	25,46	199,85	5088,2
UHMC200_1	25,00	200,5	5012,5

Table 3: Specimen geometrical data

When samples are measured the bond areas for optic fibres and strain gauges (SGs) are sanded and cleaned with acetone. The sanding serves to roughen the surface of the materials. A clean cloth with acetone is used to remove grease, oil or other residue that may compromise the adhesive when bonding fibres and SGs.

Next step is to measure up and mark the positions of the SGs and optical fibre. Some markers are dissolved by the glue which could lead to contamination in the bonding of SG and fibre. It is recommended to test the glue on a surface with the marker applied and find a marker which is not affected. Figure 11 shows the longitudinal positions of the strain gauges and optical surface fibre.
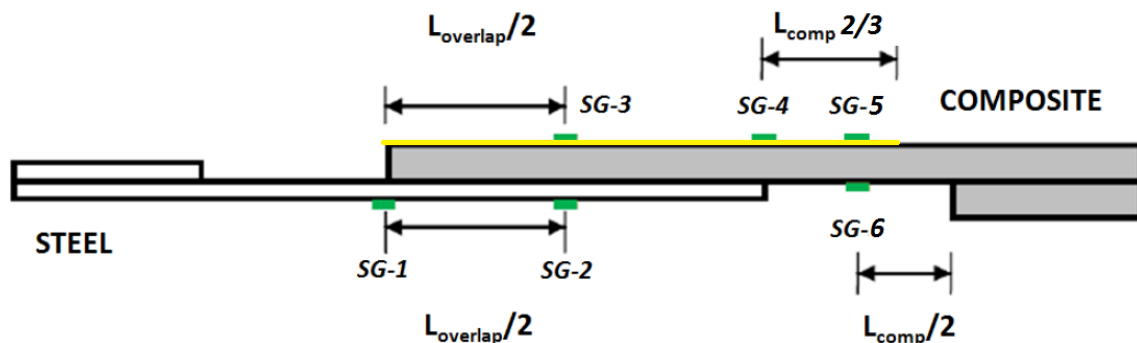
Figure 11: Position of SGs and optic fibres. From [5] modified.

The fibre and strain gauges where placed 9 mm from the outer edge of the specimen. The fibre was aligned along one edge of the laminate, and the strain gauges along the other side of

the laminate and the steel adherend. If they are installed too close to each other, they may affect each other's measurements. Some of the specimens were a bit narrower than the requested 25 mm so to spread the SGs and fibres apart the distance from the outer edge was chosen to be 9 mm instead of 10 mm. In Figure 16 the markings indicating fibre and SG positions can be seen.

3.2.2 Optical fibres

The test specimens have optical fibres embedded in the laminate with one free end exposed covered in a yellow polymer coating. This fibre is spliced with a measuring fibre which in turn is installed on the top of the laminate as indicated in Figure 11. In order to connect the fibre to the Luna OBR 4600 a pig tail has to spliced with the measuring fibre. The pig tail can be seen in the upper section of figure 16.

In order to start working with the fibres everything in Figure 12 should be in place:
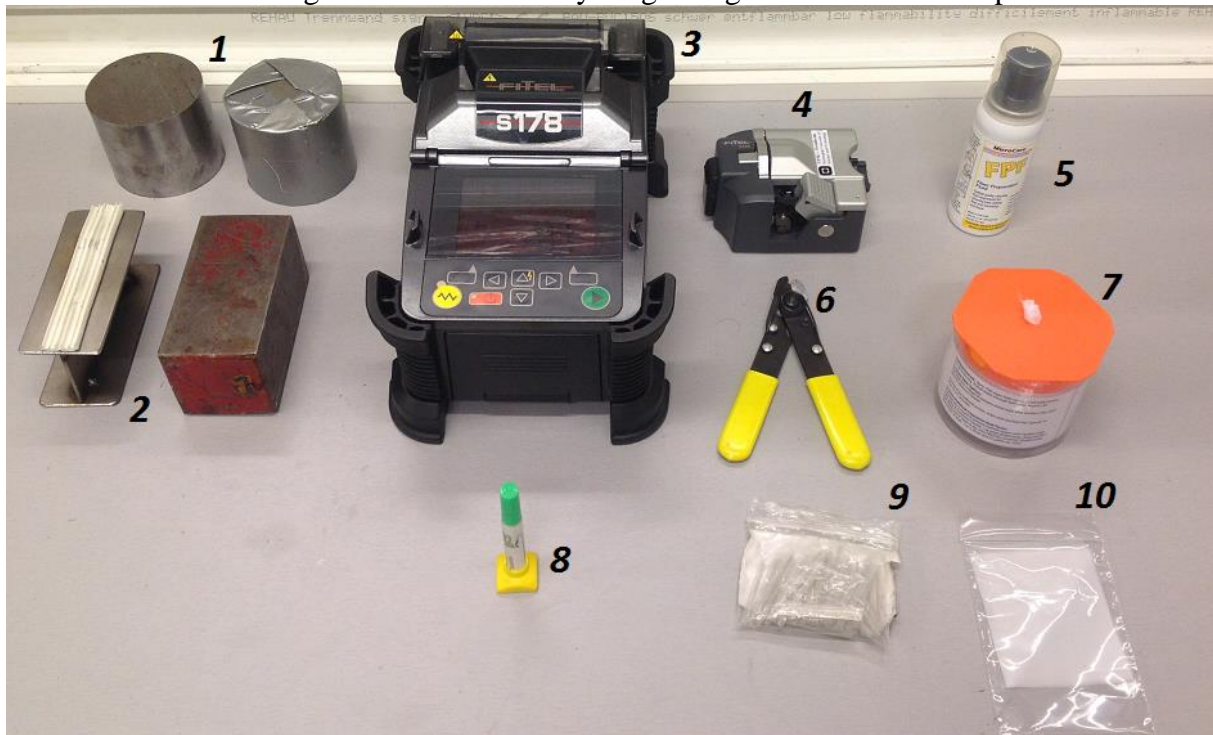
Figure 12: Overview of fibre tools: 1 support blocks, 2 pressure tool, 3 Fitel S178 fibre splicer, 4 Fitel S325 fibre cutter, 5 cleaning spray, 6 wire stripper, 7 cloths, 8 glue, 9 splice tubes, 10 Teflon sheets

The Fitel S178 is turned on, either connected to the power supply or with batteries installed. One should start working on the fibre attached to the sample. First step is to put a splice tube over the protected fibre. The coating from the fibre is removed using the wire stripper. There is glue between the protective coating and the optic fibre. If too large portions are stripped off at a time the shear strain from the glue might lead to the fibre snapping. Therefore about 10 mm in the first section should be removed and then 5 mm at a time until 25-30 mm of clear fibre is unprotected. Taking a cloth, applying some cleaning spray to it and cleaning the exposed fibre until a squeaking sound is heard is the next step. The Fitel S325 is used to cut the fibre (Figure 13) which is then placed in the S178. The fibre is secured with the clamp labelled 900-R (if on the right side of the splicer, otherwise –L if on the left) as shown in Figure 14. As seen in figure 14 the fibre should not protrude past the two needles shown in the upper left image of the figure. The first end is now ready for splicing.

10

Next step is cutting off a proper length of the thin amber coloured measurement fibre. 30-40 mm of one end is cleaned with a cloth and the spray. Then the cleaned end is burnt off with a lighter (approximately 30 mm), and the resulting soot layer is cleaned off with the fibre cloth applied with cleaning spray. When the soot is gone and the cloth gives of a squeaking sound, the fibre is ready for cutting. The fibre is then cut in the same way as previously and installed in the Fitel S178 under the clamp designated 160-L. The splicing is run. If splicing is successful the fibre is to be released from the clamps. A splice tube is slid over the joint and then placed in the heater chamber as shown in Figure 15. The spliced fibre is removed from the chamber once the cooling fan has been automatically switched off. The splice tube is still warm and if left in the chamber it might stick to the walls. It is advised to blow on the splice tube to facilitate the cool down process until the plastic turns opaque. One should now proceed to the other end of the measurement fibre.

This is prepared in the same way as the other end and secured in the Fitel S178. A splice tube is slid onto a loose pig tail and the yellow plastic coating is stripped off as before. The end is cleaned, cut and placed in the other side of the Fitel S178. When spliced and splice tube is melted over the joint, the cool down process for the splice tube is the same as mentioned above. The fibre is now ready for installation on the specimen.
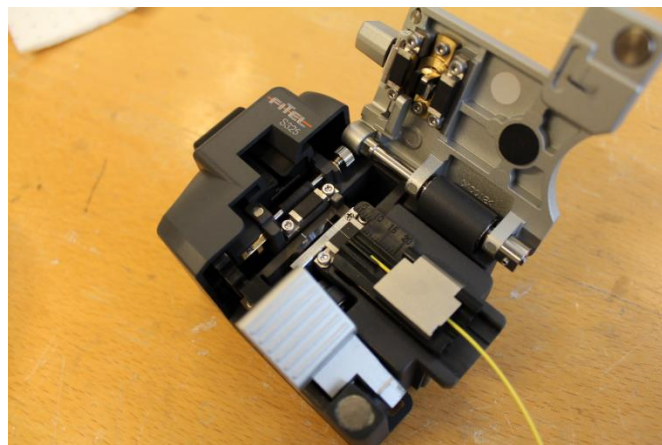
Figure 13: Cutting of fibre with Fitel S325. From [5]

Figure 14: Splicing process with S178

11
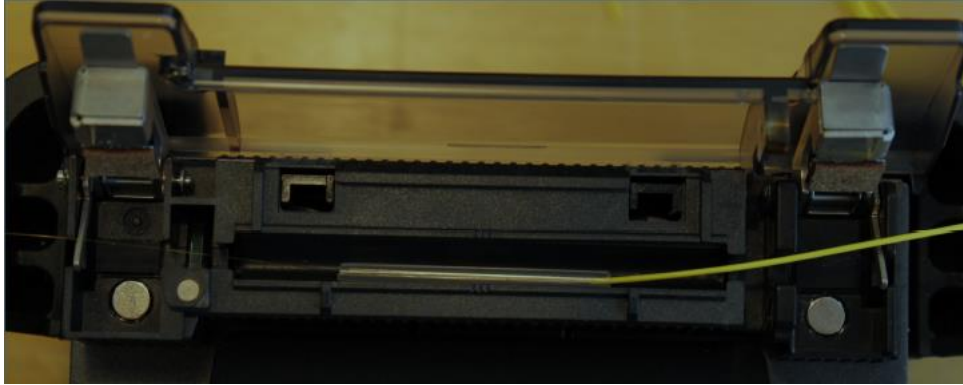
Figure 15: Splice tube and spliced fibre in heater chamber. From [5]

The portion of the fibre that will be glued to the sample is cleaned with cleaning spray to maximize the adhesion and thereby prevent noise. The fibre is aligned according to the markings on top of the laminate and secured with tape as shown in Figure 16. The specimen is placed on the support blocks and made sure to have the overlap supported, not only the tabbed ends. A Teflon sheet, glue and the pressure tool are needed next.

A thin streak of glue is applied over the fibre in a length that can be covered by the Teflon sheet. The sheet is put on top of the glue, and the white pad of the pressure tool is aligned over the sheet and fibre. Weight is now applied (Figure 17). Hand pressure is applied and kept for 1 minute.
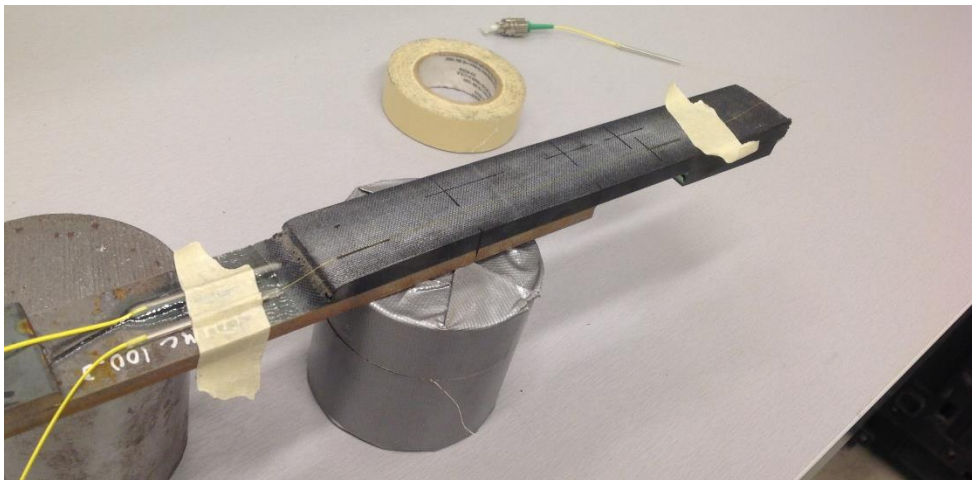
Figure 16: Fibre secured with tape. Markings indicating fibre and SG positions.
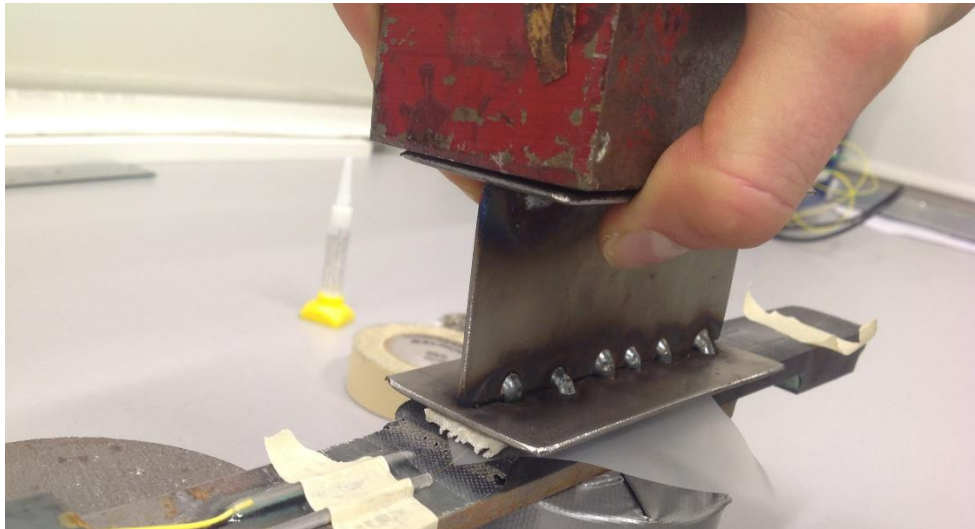
Figure 17: Gluing of fibre with pressure tool, which helps distributing pressure over the entire length

When the minute has passed, glue is applied to the next section of the fibre and the pressure procedure is repeated. If necessary fibre is secured with more tape. The measurement fibre in particular is easily damaged if pinched between sharp edges or pulled excessively. When handling the sample before testing and during installation in the test machine the fibre can easily snag onto something if not secured to the specimen.

3.2.3 Strain gauges

The specimen is suspended on the two support blocks to avoid bending the wires of the SGs when they are installed on one side. SGs are installed using the same glue as the fibre. Adhesive is applied to the bonding side of the SG which is then placed in its assigned position on the specimen. Pressure is applied for 1 minute with a Teflon sheet on top of the SG to avoid contamination of the glue and avoid spill on hands. Refer to figure 11 for positions.

3.3 Fatigue testing

3.3.1 Pre analysis

To determine the loads used during the fatigue testing, analysis of previous static testing was carried out. From the work of Lunder, E.V. (2012) [5] comparable samples to the ones tested in this project were found. In particular one sample, 3.1, had the same configuration as the HMC-samples tested during this project, although with tapered adherends. The shear strength of this sample was 12.66 MPa = τ_{max}. In order to estimate the lifetime of the fatigue specimens, in order to end up in a suitable range of life, Basquins' law was proposed:

$$\log \tau = \log \tau_0 - b \log N \qquad (1)$$

With $\tau_{max} = \tau_0$ and the constant b = 0.1, the SN curve in figure 18 could be established. In this diagram and for the following diagrams the value on the y-axis corresponds to the maximum shear stress the specimen is subjected to during fatigue testing.
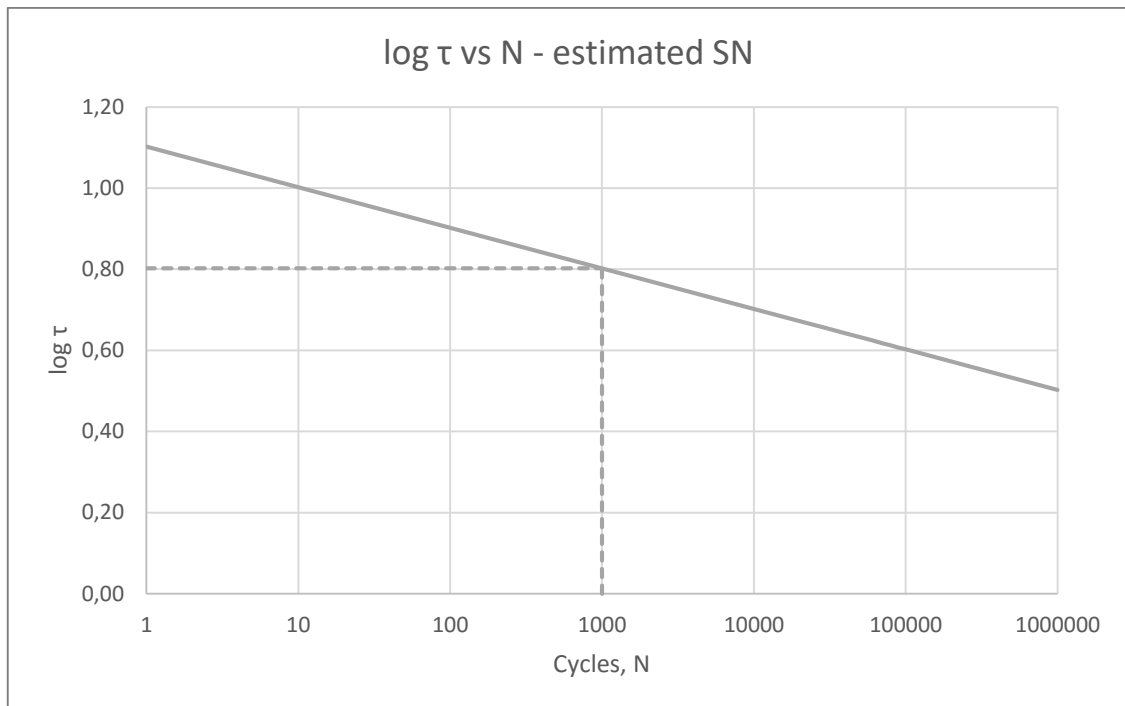
Figure 18: Preliminary SN curve

The initial SN curve is modelled by the following equation:

$$\log \tau = 1.10 - 0.1 \log N \qquad (2)$$

As a starting point a lifetime of 1000 cycles was deemed reasonable. This meant a log τ = 0.8. The loads during fatigue testing can be calculated with formula (3):

$$\tau = \frac{F}{A} \qquad (3)$$

As mentioned above the value read from the SN curve corresponds to maximum load during fatigue testing. The area is found in Table 3. During these fatigue tests an R value of 0.1 was used. For the first sample tested, HMC100_1, this corresponded to the following loads used during testing:

- Max load = 15.6 kN
- Min load = 1.6 kN
- Amplitude = 7.0 kN
- Mean load = 8.6 kN

For all the samples a frequency of 4 Hz was used. General setup of the machine is provided in the datasheet in the lab at IPM verkstedteknisk.

14

The following samples were tested during the pre-master project:

Specimen	log τ
SLJ_HMC100_1	0,8
SLJ_HMC100_2	0,9
SLJ_UHMC100_1	0,9
SLJ_UHMC100_2	0,85
SLJ_HMC100_3	0,87
SLJ_UHMC100_3	0,87

Table 4: Stress values for testing, pre-master

During the master thesis the following samples were tested:

Specimen	log τ
SLJ_HMC100_4	0,84
SLJ_UHMC100_4	0,84
SLJ_HMC200_5	0,87
SLJ_UHMC200_1	0,77

Table 5: Stress values for testing, master

3.3.2 Running of tests

The testing was performed in an Instron 100 kN machine. Initially two reference scans were performed before the lower part of the sample was clamped. Then two scans performed while pressing at the fibre at the positions corresponding to SG3 and SG4 were taken. This can be used to later find the exact point in the fibre where the SGs are positioned. The reference position for the surface fibre, later used for crack propagation analysis will also be known from this method. After these scans the specimen was clamped, and after a new scan was performed the testing could start. In order to keep track of the measurements, a spreadsheet was created where notes were taken during the test. This was necessary to keep track of the cycles and the corresponding measurement files.

Due to the use of optical fibres the fatigue test could not be run continually. The OBR scan takes a few seconds and in addition it was requested that the measurements were taken at maximum load. Therefore, manual cycling had to be utilized in the beginning. The load was increased up to max, cycled down to min, and up to max again. The fibre measurements were performed with the OBR 4600 through a Python script written by PhD candidate Sören Heinze, which automatically performed a scan and saved the corresponding file at the click of a button. After the first cycle and following scan, the manual cycling kept on until 10 cycles were reached. Once again the load was brought up to max and a scan was performed. Then down to min load and back up to mean. The reason for doing the first 10 cycles manually was uncovered during pilot testing. The Instron will at 4 Hz use longer than 10 cycles to reach full amplitudes during cycling which meant that if run automatically for the ten first cycles the specimen would not have seen the load case which it was supposed to. Since the next measurement would be carried out at 100 cycles, the effect of this would be less evident than for 10 cycles, and the sample would see several full cycles. It is worth mentioning that this is only the case during the first cycles of a test. If a test is held and then started up again, the amplitudes will be fully developed from the restart.

At this point the Instron could be programmed to event detection which could count cycles and stop when requested. Since the first 11 cycles had already been performed the first event would be after 89 cycles. When the event was reached, the same procedure of loading to max, performing measurement, unloading to min and up again to mean was performed. This meant that an additional cycle had been performed and the next event would not be after 100 new cycles, but after 99. In other words, the next event was at 188 cycles. The use of a spreadsheet and handwritten notes to keep track of the events is recommended. The scans were taken further apart throughout the testing.

In addition to programming the Instron for events and performing fibre scans it was necessary to inspect the sample for crack initiations. Both sounds and visual inspection was utilized and notes were taken. Initially there was not a complete protocol for gathering data during testing. Some of the early experiments therefore have a lack of data from visual inspection, however initiation of the crack was in most cases detected.

3.4 Data analysis

3.4.1 Strain gauges

The information provided by the strain gauges is not directly used for the crack growth analysis. Compared to the fibre the strain gauges will give data for one point on the specimen only. This will be used to compare the strain values of the optic fibre in the same location (see section 3.3.2) in order to verify the results.

The data from the analysis is imported into SciDaVis. A plot of load vs time gives a picture of the experiment load history. The horizontal sections of the graph, where the load is held constant, is where the OBR measurements are taken. This can be seen in figure 19. The data reader is highlighting the point of interest and makes it possible to read out the time at this instant. The corresponding value from the strain gauge at this point in time is then compared with the OBR data file.
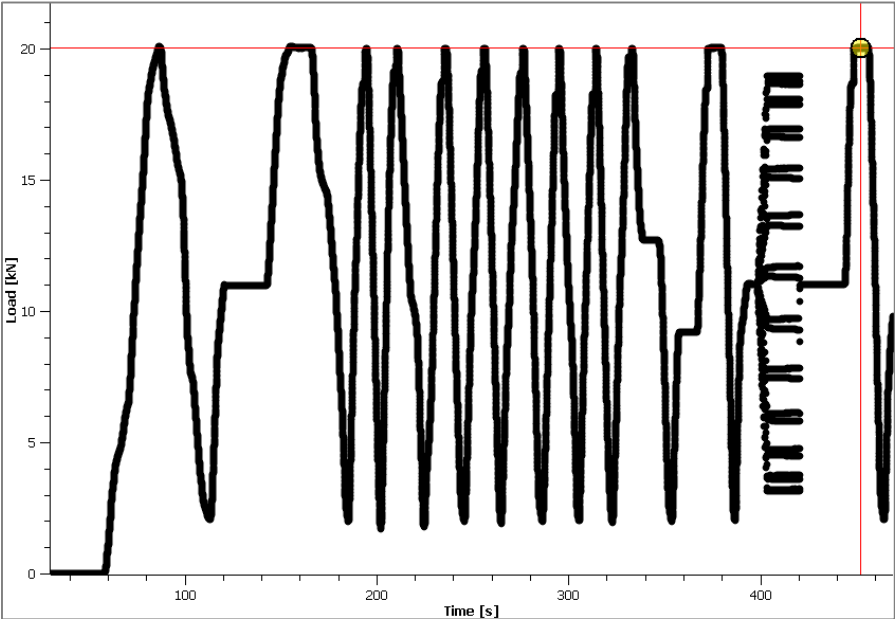
Figure 19: Force vs time plot showing at which point in time to pick strain gauge value. This example is after 100 cycles.

3.4.2.1 OBR analysis overview

When performing the fibre analysis, only one measuring fibre is used per specimen. The configuration is according to figure 20 and the position of the measuring points within the fibre follows the direction indicated by the arrows; from the composite tab end, through the loop and back towards the composite tab again.
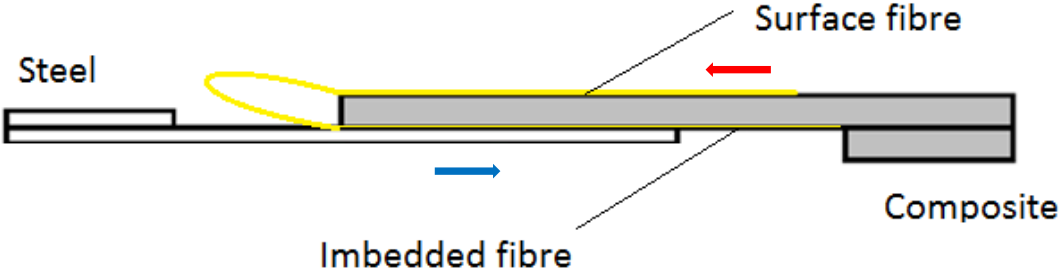
Figure 20: Optic fibre direction. Red direction for the surface fibre and blue direction for the embedded fiber

The crack will form in the point indicated in figure 21, and propagates in the direction indicated by the arrow. This means that the position of the crack tip will propagate in the negative direction for the surface fibre, and in the positive direction for the embedded fibre.
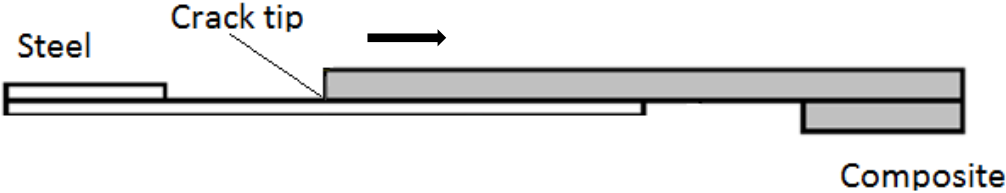
Figure 21: Direction of crack propagation

The direction of growth can be seen in figures 22 and 23 below. The bath tub curve can also be recognized in figure 22.
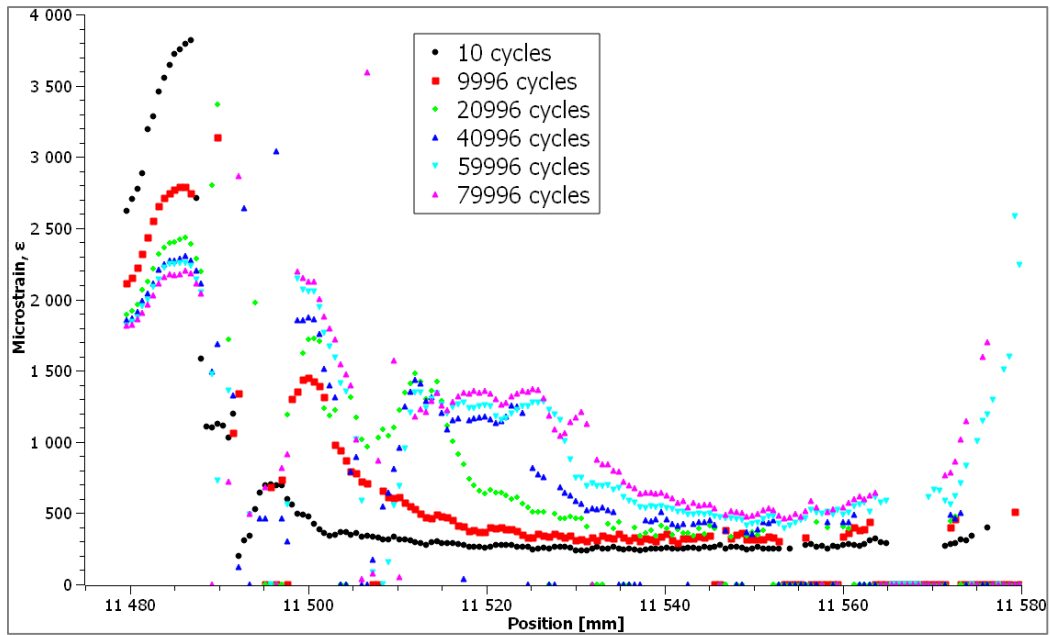
Figure 22: Overview of crack propagation in SLJ_HMC100_1, embedded fibre
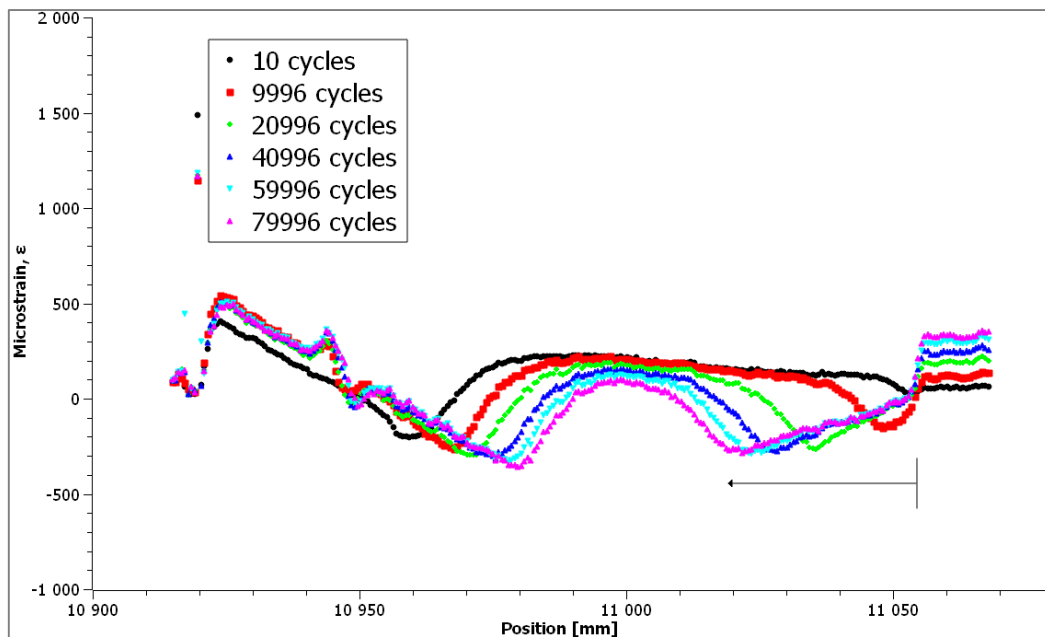
Figure 23: Overview of crack propagation in SLJ_HMC100_1, surface fibre

The plots are made in the program SciDaVis. The data reader tool makes it possible to pick out the exact data point of interest for each measurement.

3.4.2.2 Crack initiation – embedded fibre

In order to find the crack initiation, data from both the embedded fibre and the surface fibre has been used. The embedded fibre shows the internal strain field in the overlap and will in most cases provide good data.

When tracking the initiation with surface fibre the first objective is to plot an overview picture of strain vs position for a few OBR measurements spread out during the experiment. The plots

18

will travel like waves along the x-axis when the crack propagates. This can be seen in the figure 22 above. From the overview it can be approximated at which number of cycles the crack starts to grow. A new plot is made with measurements surrounding the area of interest. This is repeated until the measurement where the crack starts has been isolated. Jumps and/or movements of the peaks are signs of an opening crack. Keeping one measurement with a low cycle count is useful to keep track of the initial situation.

3.4.2.3 Crack initiation – surface fibre

For the surface fibre the starting point of the overlap is more evident from the measurements. In addition the position of the surface fibre is known due to the position calibration of the strain gauges as noted in section 3.3.2. The strain gauge SG3 will be positioned in the middle of the overlap as indicated in figure 11, and from this, the end of the overlap is possible to find. The position of the SG will not be completely accurate for each case due to small inaccuracies when gluing and differences in overlap length, therefore the position is verified with the graphical data.

As seen in figure 23, the measurements are narrowing down the starting point of the crack by following the valley backwards to the point of origin. Plots are made with measurements surrounding the area of interest until the valley has its first shift in position, which is recorded as the initiation.

3.4.2.4 Crack growth – embedded fibre

The crack front is followed from the point of initiation and the overview shown in figure 22 is beneficial to see which area of the curve to keep track of. Some plots are made with only one measurement, others with several, in order to follow the tip. The peak positions are tracked and recorded against the number of cycles.

3.4.2.5 Crack growth – surface fibre

In the same was as for the embedded fibre the crack starts at the initiation. The valley positions are tracked and recorded against the number of cycles.

4 Results

4.1 Failure

The first sample tested during the fall of 2015 ended up exceeding the expected life of 1 000 cycles, estimated in 3.3.1. It was decided to stop the test after 102 000 cycles when failure still had not occured. Calculating the lifetime of the sample based on the later test results, given by equation (4), the expected life would be close to 1 500 000 cycles. If calculating by the SN curve for the HMC samples only, equation (5), the result would be around 700 000 cycles. The initial estimate of life was clearly on the conservative side. The adjustments made to the load after the initial test gave good results, which are all shown in Table 6.

Compared to the 100 mm samples, the 200 mm samples did not have static testing data available. The first tested, the HMC200_5 was expected to end early in the fatigue range and thus the load was set high, but failed already during the first loading up to max. Adjustments were made to the second specimen by reducing the maximum load to 80% which reflects in the logarithmic stress value as a reduction from 0,87 to 0,77. Yet again, the sample failed before completing a full cycle.

Sample	N	log T	Comment
HMC100_1	102000	0,8	Excluded from regression due to test stopped before failure
HMC100_2	1424	0,9	
HMC100_3	19626	0,87	
HMC100_4	57879	0,84	
UHMC100_1	5882	0,9	
UHMC100_2	39594	0,85	
UHMC100_3	23990	0,87	
UHMC100_4	38051	0,84	
HMC200_5	0	0,87	Failed on first loading before completing 1 cycles
UHMC200_1	0	0,77	Failed on first loading before completing 1 cycles

Table 6: Failure due to fatigue

The 200 mm samples did not provide any data for further analysis and is therefore not featured in the SN curve nor the strain field analysis.

For the 100 mm samples the SN Curve established through testing ended up as:

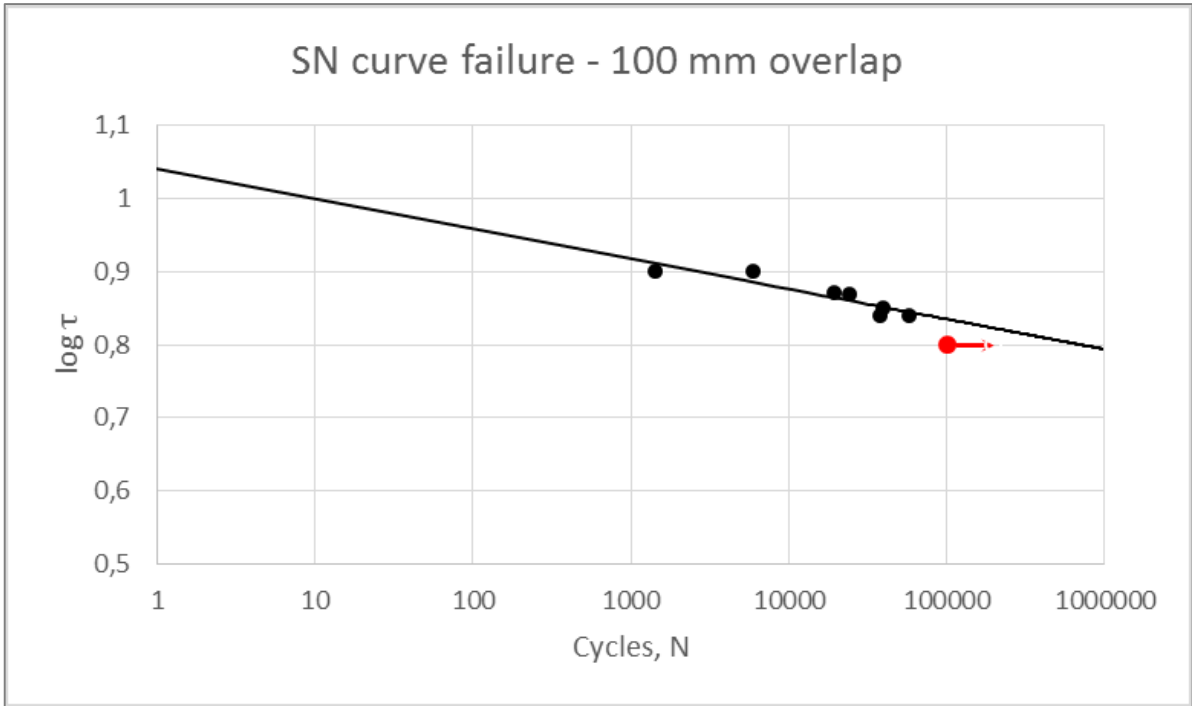$$\log \tau = 1.042 - 0.041 \log N \tag{4}$$

Figure 24: SN curve of failure

The SN curve in Figure 24 is plotted with the results, excluding the runout HMC100_1, which was stopped before failure could occur. The regression line through the points is what gives the constants in equation (4). The $\tau_0 = 1.042$ is compared to 1.10 for the initial and $b = 0.041$ vs 0.1. The value of τ_0 is related to the static failure of the joint. The joint tested during fatigue did not have the exact same geometry as the tapered one, which could explain the difference. The tapering of the adherends should increase the joint strength as mentioned in 2.2.2., which could explain why the fatigue samples show a different behaviour. The lack of data points in the area below 1 000 cycles could be another reason.

The slope of the curve, on the other hand, is flatter than the initial estimate. This means that for a reduction in load the increase in lifetime will be better compared to samples having a higher value of b.

Another plot was also made comparing the HMC with the UHMC as can be seen in figure 25 below. The HMC samples appear to have a flatter SN curve, but the value of this data is limited due to the small number of test results.
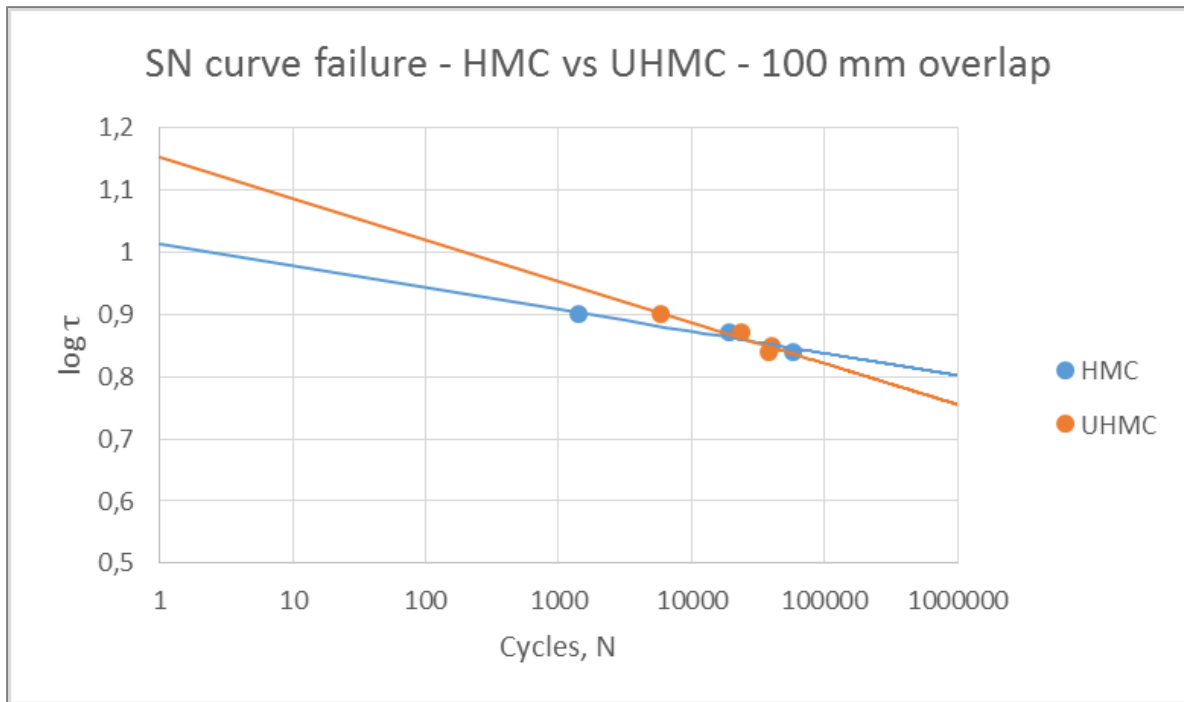
Figure 25: SN curve of failure comparing HMC and UHMC

SN Curve for HMC is given by:

$$\log \tau = 1.014 - 0.035 \log N \qquad (5)$$

SN Curve for UHMC is given by:

$$\log \tau = 1.151 - 0.067 \log N \qquad (6)$$

The failure modes for the samples were delamination, debonding and fibre fracture, which coincides with the conclusions in [6]. Some pictures of the crack surfaces are shown in figures 26 and 27. In figure 26 there is a clear delamination running the entire length of the overlap. This is in agreement with what can be seen in figure 4. In figure 27 there are both signs of fibre fracture and adhesive failure, where the latter can be seen on the steel in form of debonding. In figures 28 and 29 delamination and debonding can be seen.

Figure 26: Failed sample HMC100_4 showing delamination

Figure 27: Failure in UHMC100_4 showing delamination, clear debonding of adhesive layer and fibre fracture.

4.2.1 Crack initiation – visual

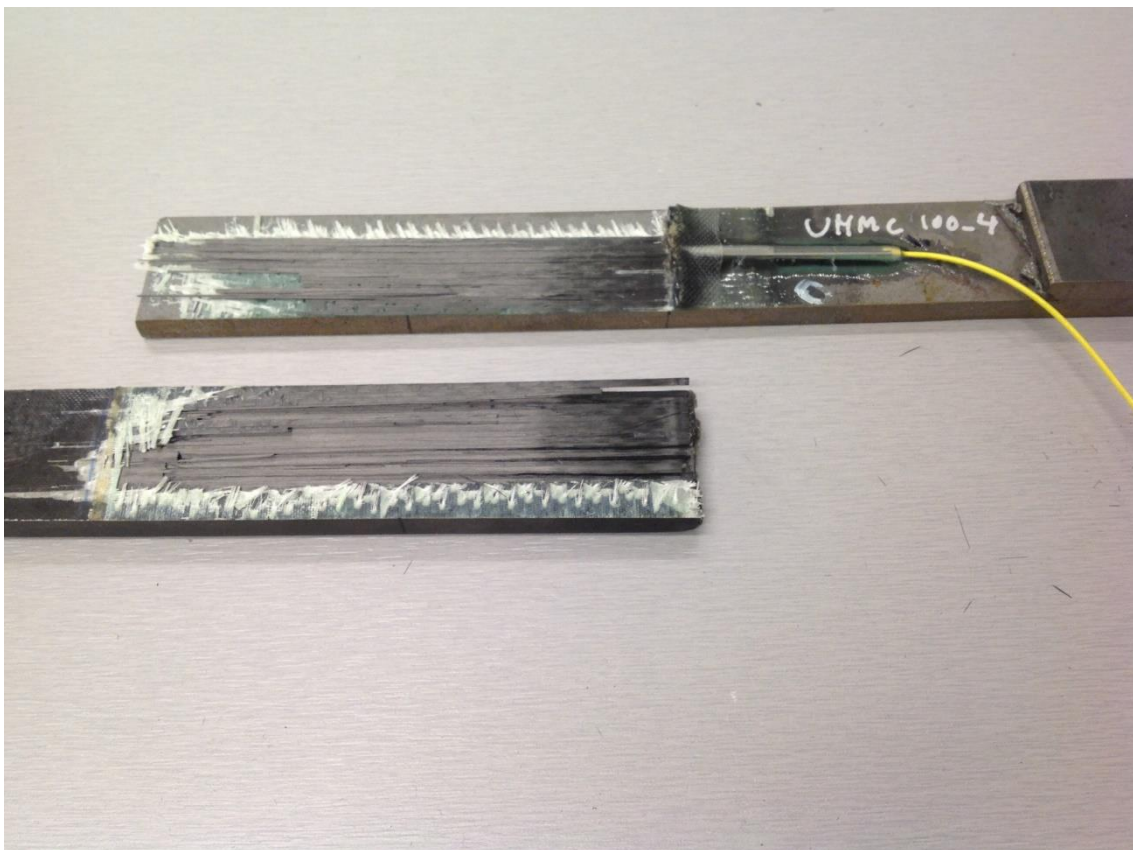When investigating the specimens during cycling the cracks often appear as debondings on one side and as delaminations on the other. In figure 28 it can be seen that sample HMC100_2 is showing delamination on one side and what started as debonding on the other side and progressed into interlaminar delamination during failure. It was not possible to take good pictures during the experiment.

Figure 28: HMC100_2 with delamination in the left, and debonding progressing to delamination on the right

Figure 29 shows the failed specimen UHMC100_3 having delamination on one side, and delamination and debonding on the other. Most failures cracks started simultaneously as debonding on one side and delamination on the other. The delamination of the debonding side usually continued within the laminate from a distance equalling the crack tip of the debond. This is what is referred to as interlaminar failure in figure 7.
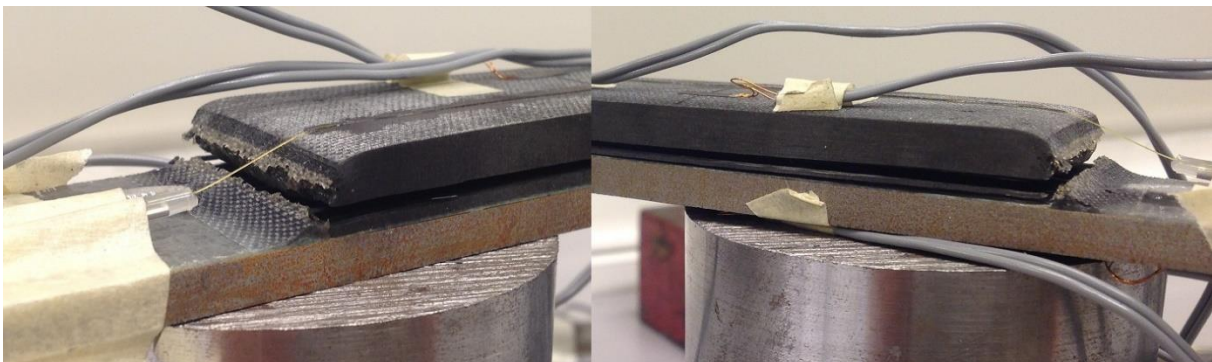

Figure 29: UHMC100_3 with delamination on the left, and debonding and delamination on the right

In addition to cracks developing on the composite side, there were also debonding from the end of the steel adherend. These always developed later than the ones from the composite side and have therefore not seen any focus at this time. An example from sample HMC100_3 can be seen in Figure 30.

Figure 30: Debonding of steel adherend in HMC100_3

Visual crack initiation results are shown in table 7. In sample UHMC100_1 the initiation of the crack was considered caught too late and is therefore not included.

Sample	N	log τ	Comment
HMC100_1	10000	0,8	
HMC100_2	350	0,9	
HMC100_3	1000	0,87	
HMC100_4	8100	0,84	
UHMC100_1		0,9	Did not catch start
UHMC100_2	5500	0,85	
UHMC100_3	50	0,87	
UHMC100_4	1300	0,84	

Table 7: Crack initiation – visual detection
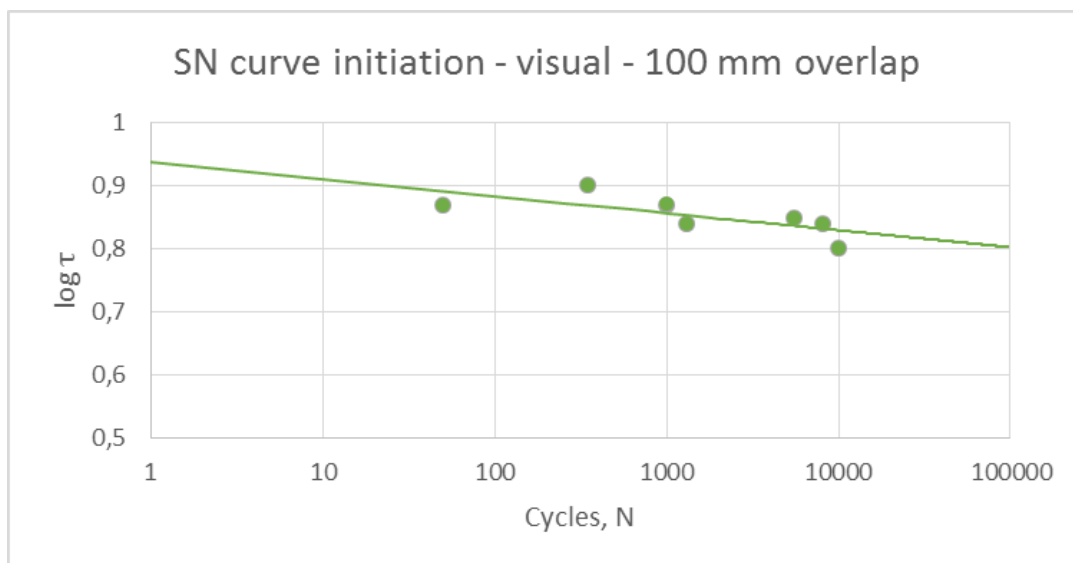
SN curve for visual initiation is plotted in Figure 31.

Figure 31: SN curve of crack initiation - visual

25

SN Curve for visual crack initiation is given by:

$$\log \tau = 0{,}938 - 0{,}028 \log \mathrm{N} \qquad (7)$$

4.2.2 Crack initiation – embedded fibre

Following the procedure of section 3.4.2.2 gave a good starting point for the initiation analysis. The exact location of the crack growth is difficult to assess. As seen in figure 32, the peak starts to grow in y-direction and eventually moves in the x-direction when crack initiates. The peak grows narrower towards the top and in some cases the peak is not easy to distinguish. In figure 32 the initiation can be seen as a jump and a shift in the peak.
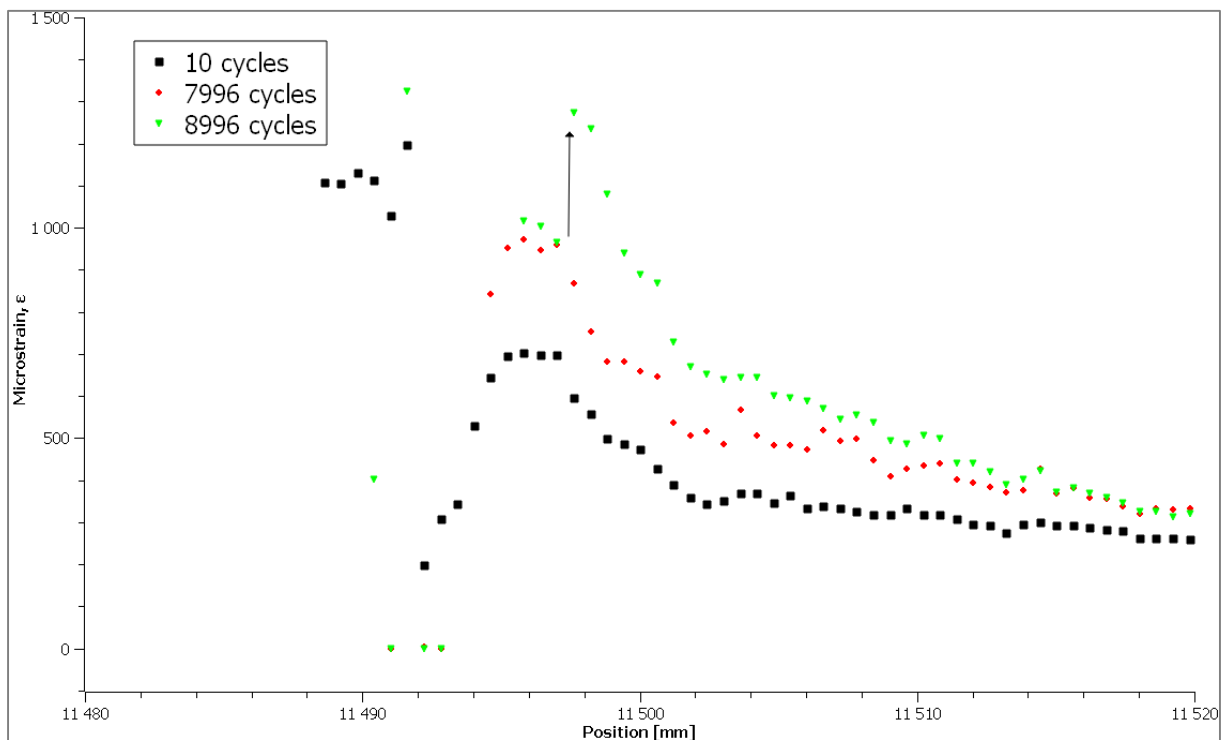
Figure 32: Crack initiation in SLJ_HMC100_1 by method of embedded fibre

The same procedure is used for the rest of the samples and the number of cycles for crack initiation is recorded. Results are shown in table 8. In two of the samples initiation was not recorded. In Appendix A.3, figure 75 shows an example of noise problems in sample HMC100_3.

Sample	N	log τ	Comment
HMC100_1	8996	0,8	
HMC100_2	400	0,9	
HMC100_3		0,87	OBR-file noise
HMC100_4		0,84	OBR-file noise
UHMC100_1	100	0,9	
UHMC100_2	200	0,85	
UHMC100_3	100	0,87	
UHMC100_4	600	0,84	

Table 8: Crack initiation – OBR embedded fibre detection

26

SN curve for crack initiation from embedded fibre is shown in figure 33:

Figure 33: SN curve of crack initiation - embedded fibre

SN curve for crack initiation by method of embedded fibre is given by:

$$\log \tau = 0,969 - 0,041 \log N \tag{8}$$

4.2.3 Crack Initiation – surface fibre

As seen in figure 3 the specimen will deform in such a way that the top surface will curve. During testing the whole specimen will be tensioned but the curvature gives a reduction in the surface tension appearing as valleys in surface fibre measurements. The initiation of sample HMC100_1 can be seen in figure 34. The vertical line plotted is at a distance of 50 mm from SG3, as mentioned in the procedure in 3.4.2.2. In this case, the position coincides with the graphical data.
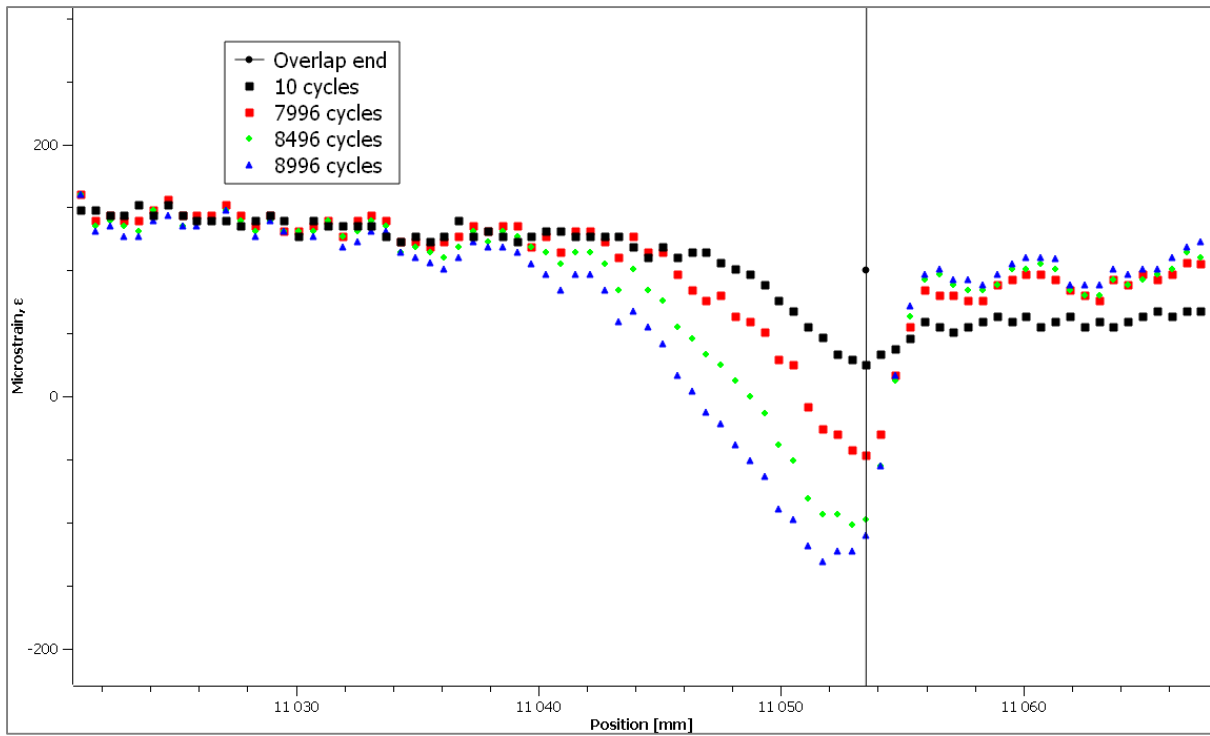
Figure 34: Crack initiation in SLJ_HMC100_1 by method of surface fibre

Following the same procedure for all the samples provides results shown in table 9.

Sample	N	log τ	Comment
HMC100_1	8496	0,8	
HMC100_2	400	0,9	
HMC100_3	600	0,87	
HMC100_4	10000	0,84	
UHMC100_1	10	0,9	
UHMC100_2	100	0,85	
UHMC100_3		0,87	OBR-file noise
UHMC100_4	500	0,84	

Table 9: Crack initiation - OBR surface fibre detection

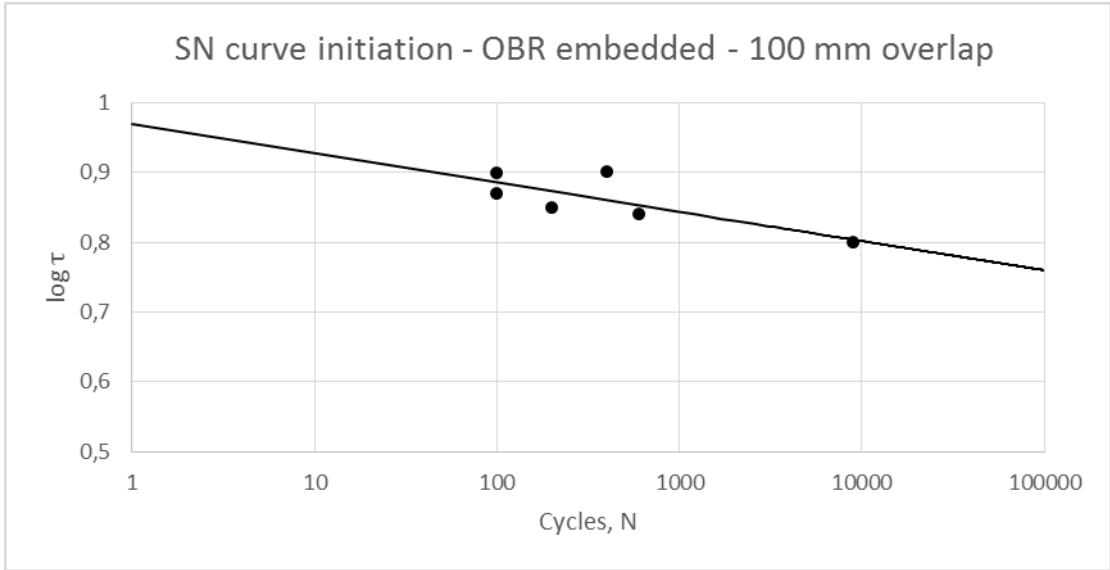SN curve for crack initiation from surface fibre is shown in figure 35.
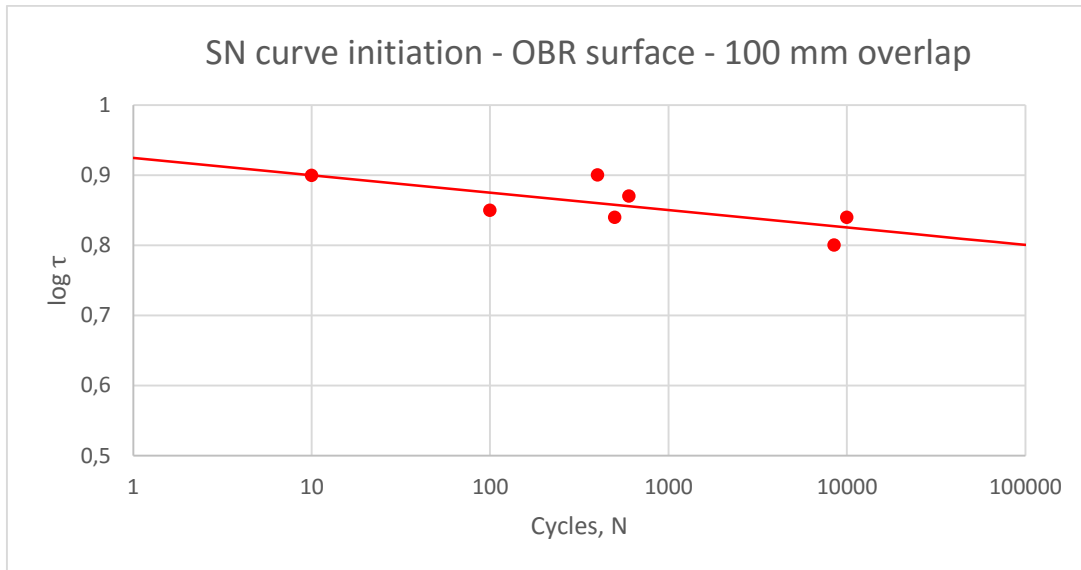
Figure 35: SN curve of crack initiation - surface fibre

SN curve for crack initiation by method of surface fibre is given by:

$$\log \tau = 0{,}925 - 0{,}025 \log N \qquad (9)$$

4.2.4 Crack initiation – comparison

To get a visual overview of the initiation the three methods are compared in figure 36. The slope of the initiation for the embedded curve is steeper than the other two, however, this one has two missing results which gives more uncertainty when plotting the SN curve.

Figure 36: SN curve comparison

29

The results are summarized in table 10. Fibre measurements appear later because they can only be performed at a given number of cycles and not continually like the visual.

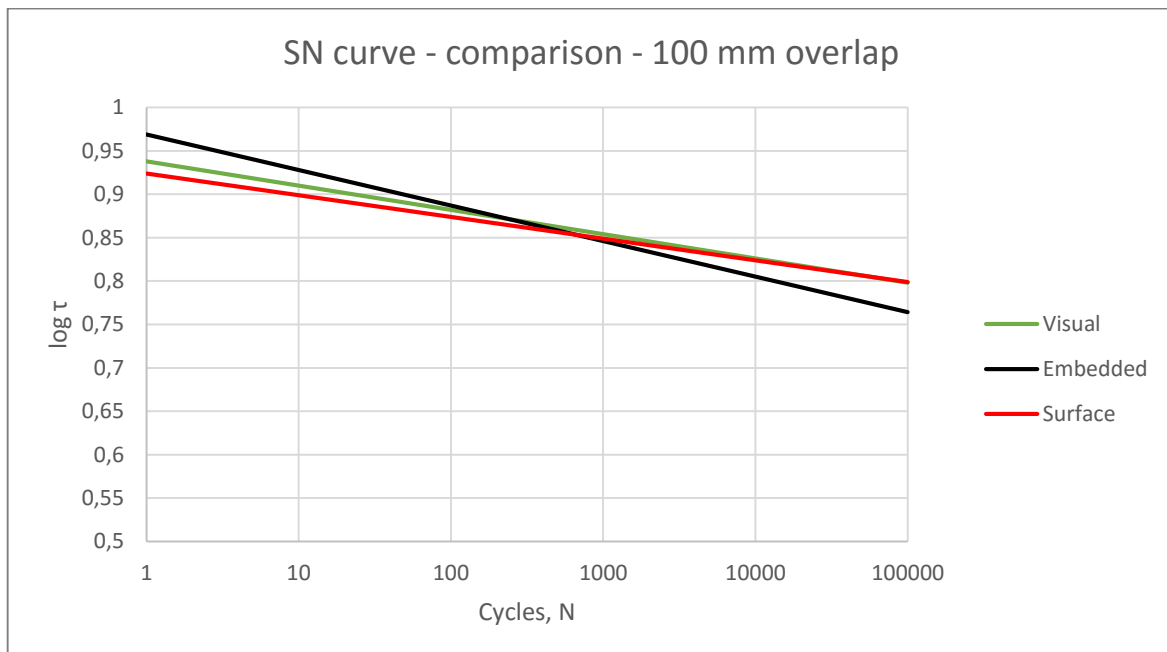| Sample	Visual N	Embedded N	Surface N	log τ
HMC100_1	10000	8996	8496	0,8
HMC100_2	350	400	400	0,9
HMC100_3	1000		600	0,87
HMC100_4	8100		10000	0,84
UHMC100_1		100	10	0,9
UHMC100_2	5500	200	100	0,85
UHMC100_3	50	100		0,87
UHMC100_4	1300	600	500	0,84

Table 10: Crack initiation summarized

4.3 Crack propagation

4.3.1 Crack propagation – embedded fibre

Figure 37 shows crack propagation for sample HMC100_1 between 10 996 cycles and 30 996 cycles. At the lifespan shown the measurements are taken 10 000 cycles apart which gives the crack time to grow. The shift of the peaks, as indicated by the arrows, are an indication of crack propagation.

Figure 37: Crack propagation in SLJ_HMC100_1 by method of embedded fibre. Arrows highlighting peak front.

Plots for crack length vs number of cycles are found in section 4.3.3. In addition, figures showing da/dN vs number of cycles are also presented.

4.3.2 Crack propagation – surface fibre

Figure 38 shows crack propagation measured with surface fibre for HMC100_1. To give a clear overview only 3 measurements are shown. The shift of the valleys, indicated by arrows, are an indication of crack propagation.
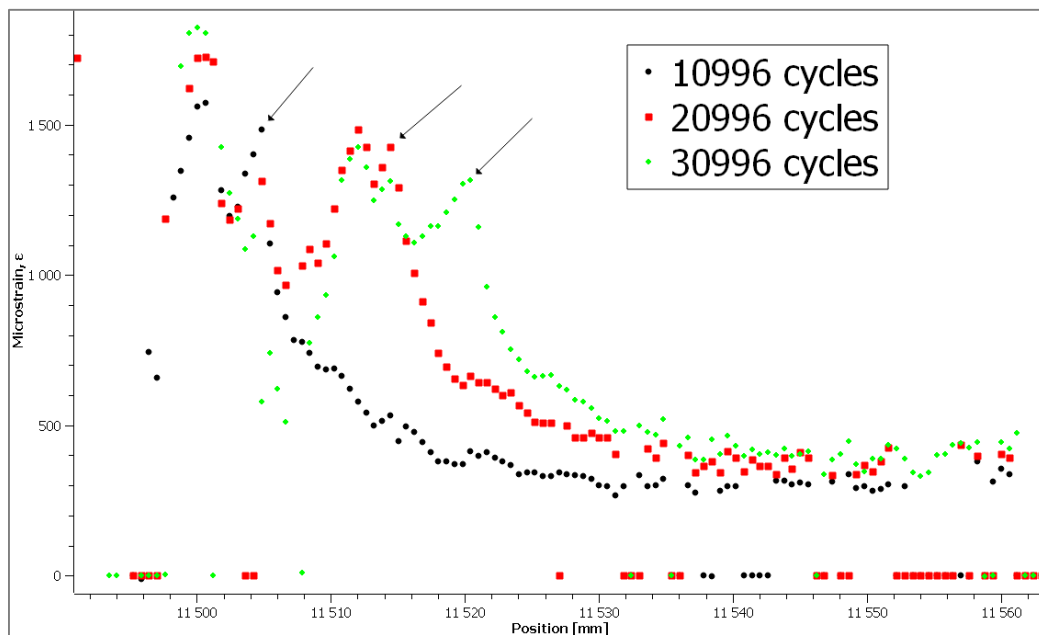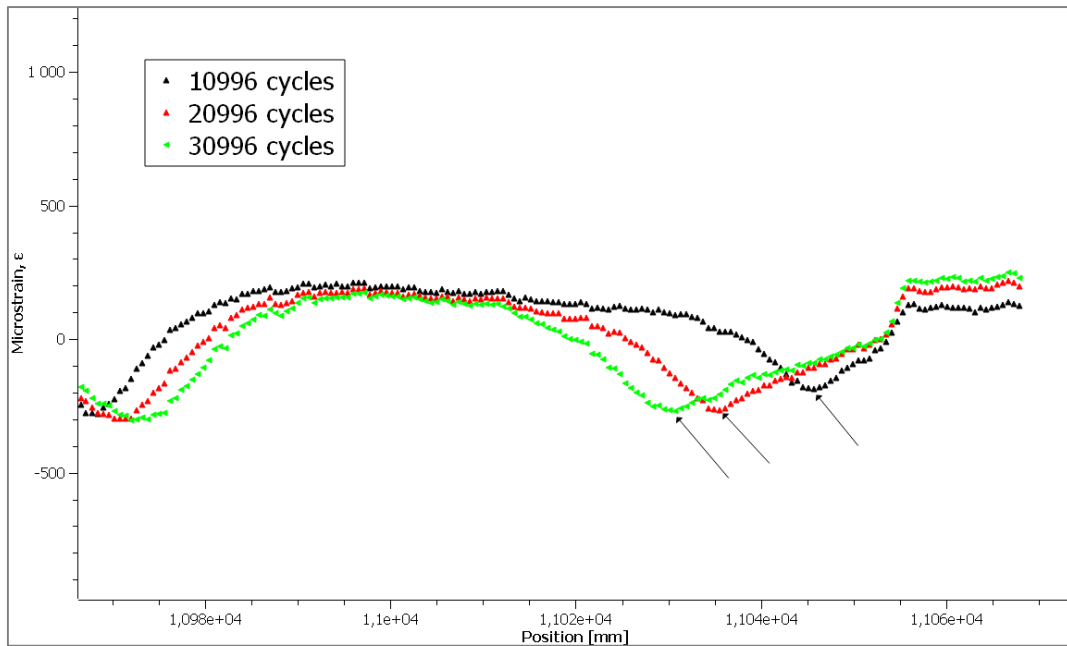
Figure 38: Crack propagation in SLJ_HMC100_1 by method of surface fibre. Arrows highlighting peak front.

Plots for crack length vs number of cycles are found in section 4.3.3. In addition, figures showing da/dN vs number of cycles are also presented.

4.3.3 Crack propagation – comparison and plots

Table 8 and 9 show which samples have usable data for crack initiation and that also carries over to crack propagation. There are two missing observations for the HMC samples and two missing for the UHMC samples. For each sample both propagation from embedded fibre and from surface fibre are shown in the plot, but due to the aforementioned some plots are with one method only.

There are two plots shown for each sample:
- Crack length vs log N
- da/dN vs log N

In appendix A.2 the following plots can be found in figures 59 to 74:
- Crack length vs N
- da/dN vs N

31

In figure 39 and 40 sample HMC100_1 is presented. After crack initiation at around 8500-9000 cycles the crack grows at a high rate to a little over 10 000 cycles as indicated by the da/dN plot in figure 40, before crack rate reduces. At 40 000 cycles the crack has reached a stable level. There were no good measurements after 80 000 cycles but from figure 39 the crack had only reached between 30-35 mm which indicates that failure is not in the near future. The HMC100_1 was stopped after 102 000 cycles. There is correlation in the crack growth but some deviance in the early phases between surface and embedded fibre.
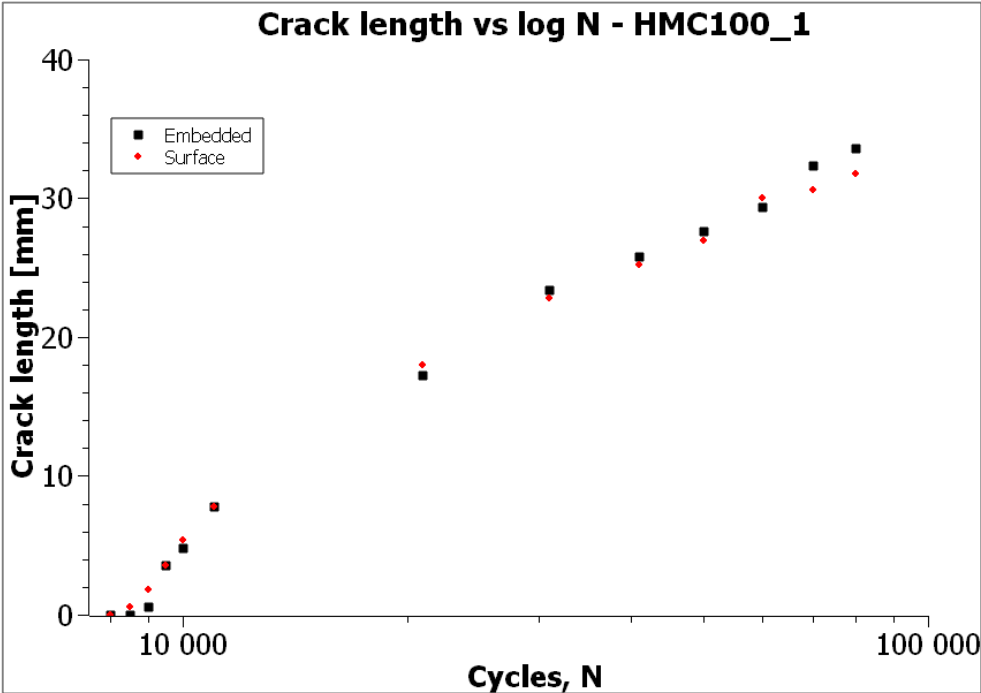
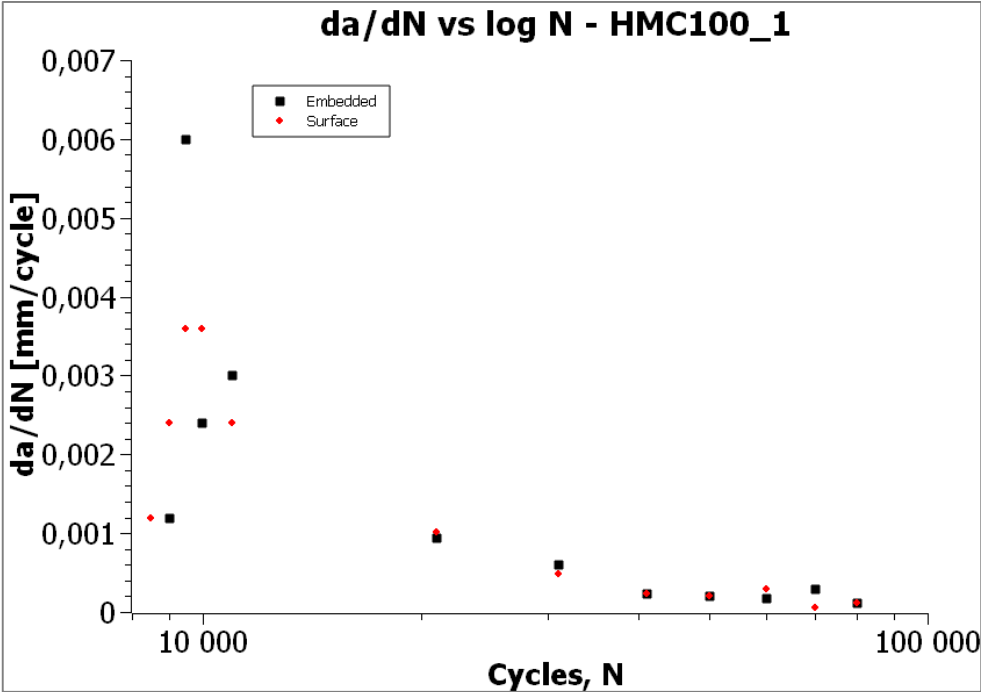

Figure 39: Crack length vs log N for HMC100_1

Figure 40: da/dN vs log N for HMC100_1

32

Figure 41 shows crack propagation of sample HMC100_2. This sample was tested in the high end of the spectrum with a log τ = 0,9. Crack initiation was late considering the load. It happened at 400 cycles, which for this sample was abrupt and with a large and audible crack opening. Compared to some of the other samples the initiation was late when considering the load. As seen in figure 42 the crack growth was stable but at a very low rate compared to the opening and ending rate. When 1200 cycles was reached it accelerated towards failure. Embedded fibre and surface fibre give quite similar results. One measurement file was missing for the embedded fibre.
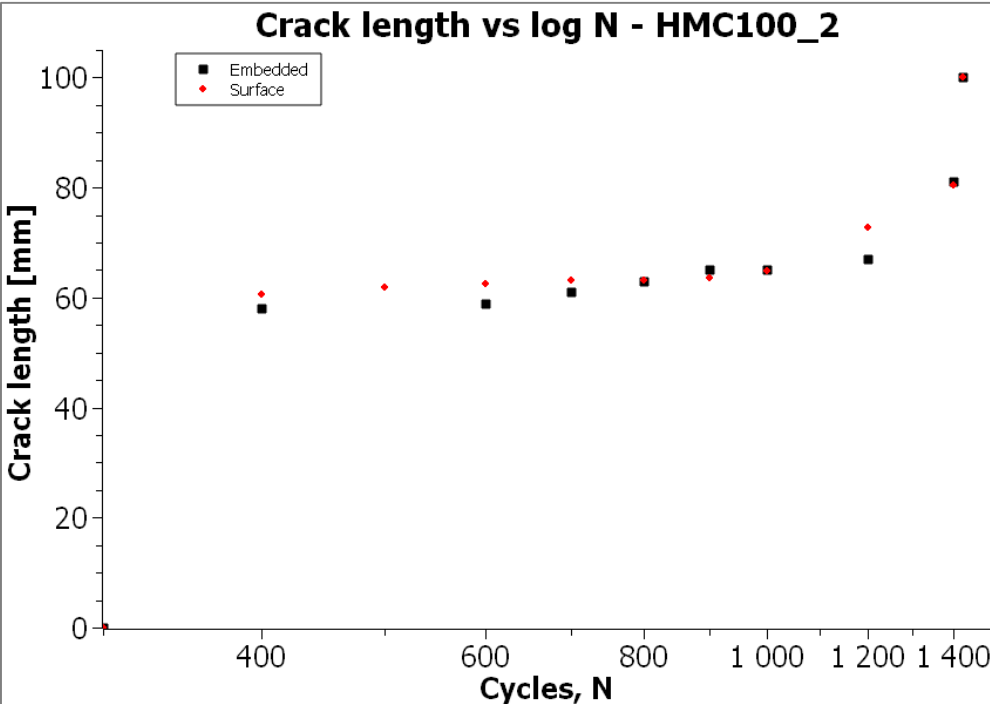
Figure 41: Crack length vs log N for HMC100_2
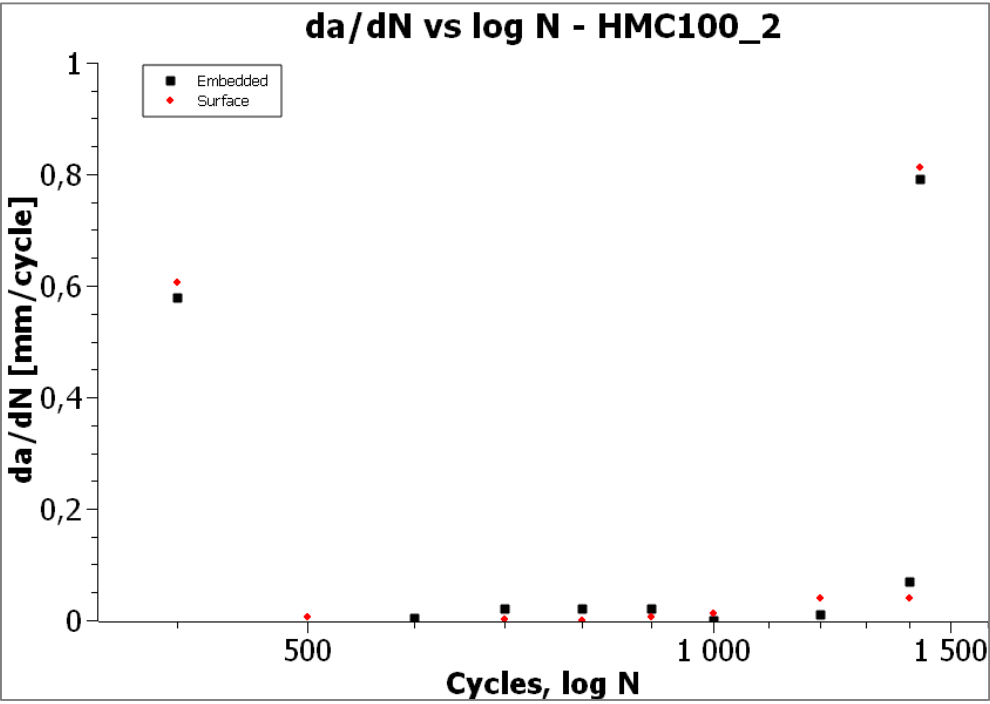
Figure 42: da/dN vs log N for HMC100_2

Sample HMC100_3 can be seen in figures 43 and 44. In figure 44 some jumps in crack growth are picked up in the early phases. Overall, the growth seems fairly linear after about 1000 cycles although with some local plateaus. Early initiation and several measurements gives many data points which help creating a good plot of the crack length.
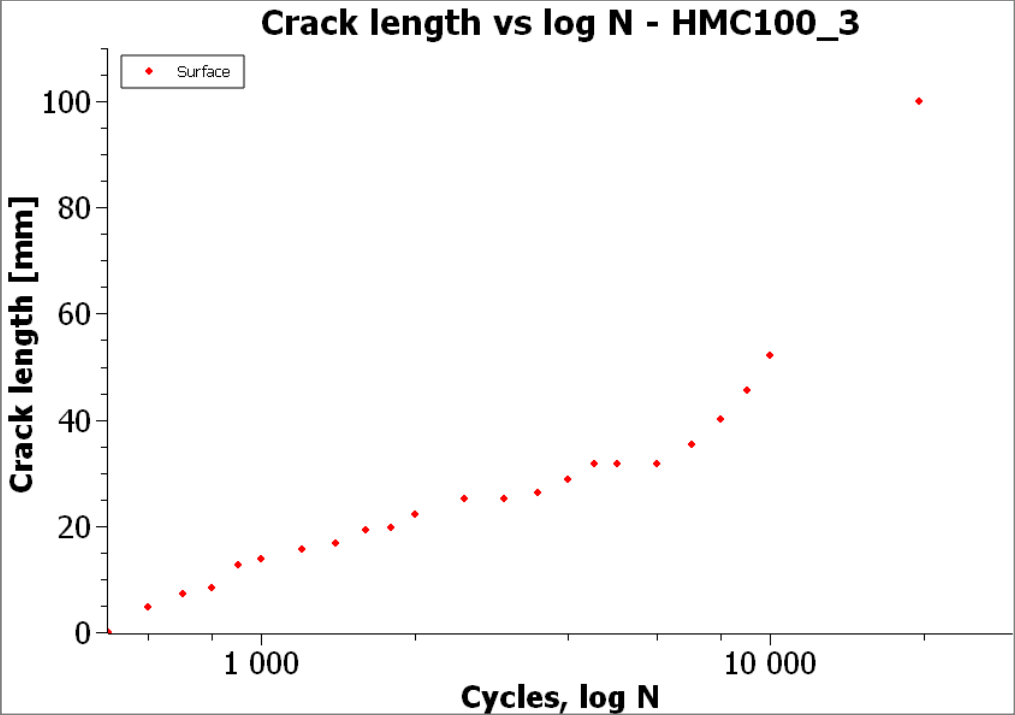
Figure 43: Crack length vs log N for HMC100_3
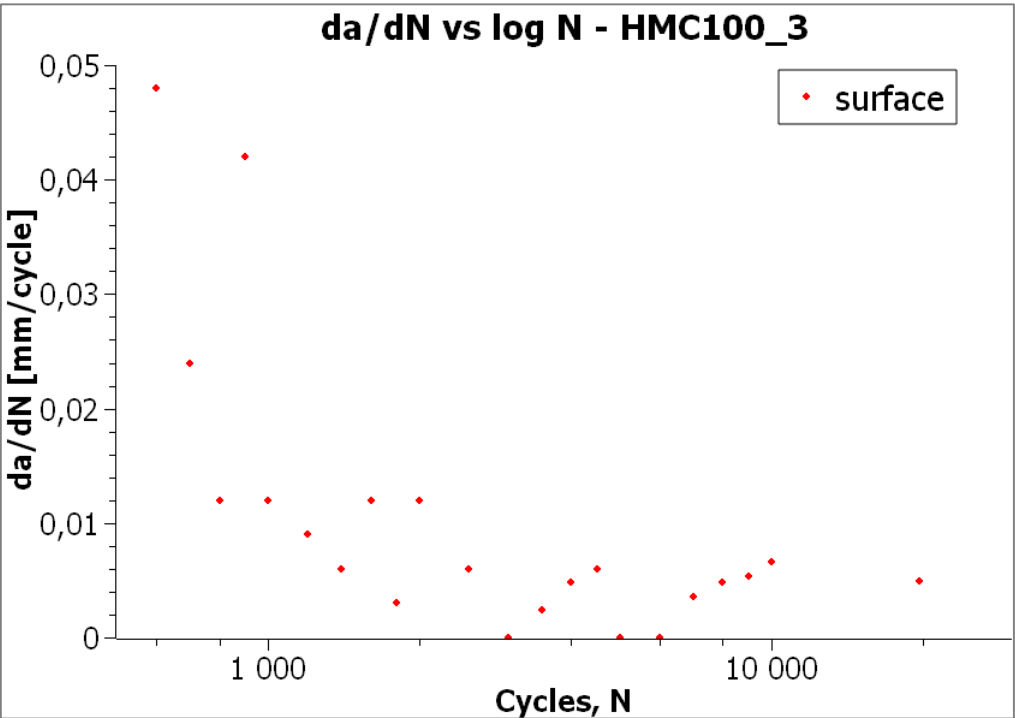
Figure 44: da/dN vs log N for HMC100_3

HMC100_4 was the other sample providing only surface measurements, shown in figures 44 and 45. The initiation was late and the measurements were therefore fewer in numbers than most of the other samples. A higher rate of growth in the beginning and towards the end. The low measurement number gives an unprecise picture of the growth in the middle section.
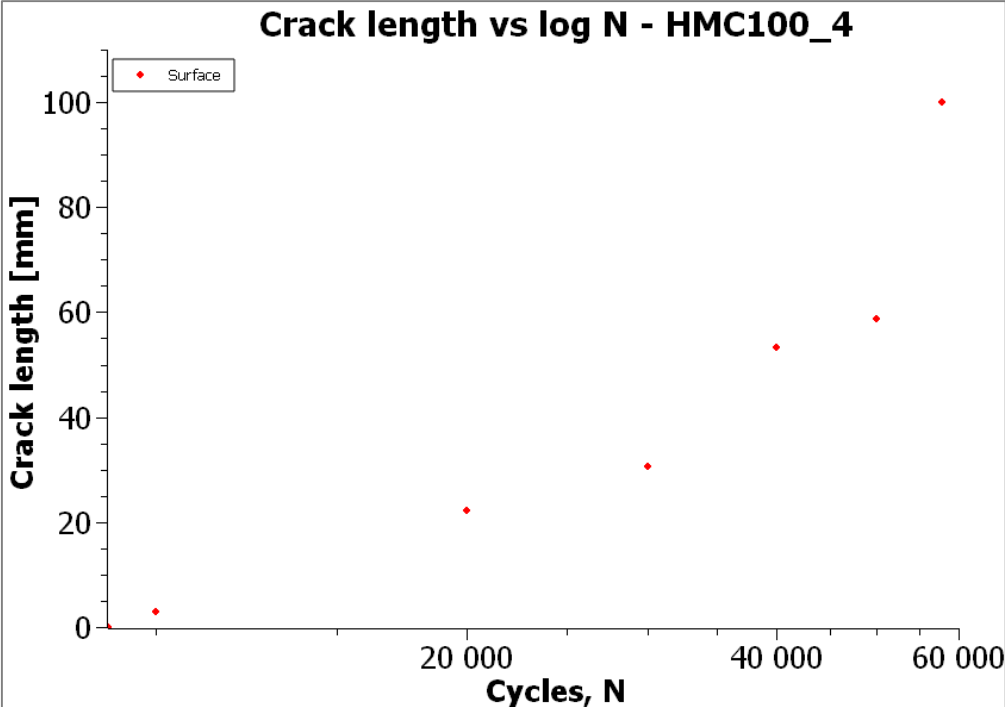
Figure 45: Crack length vs log N for HMC100_4
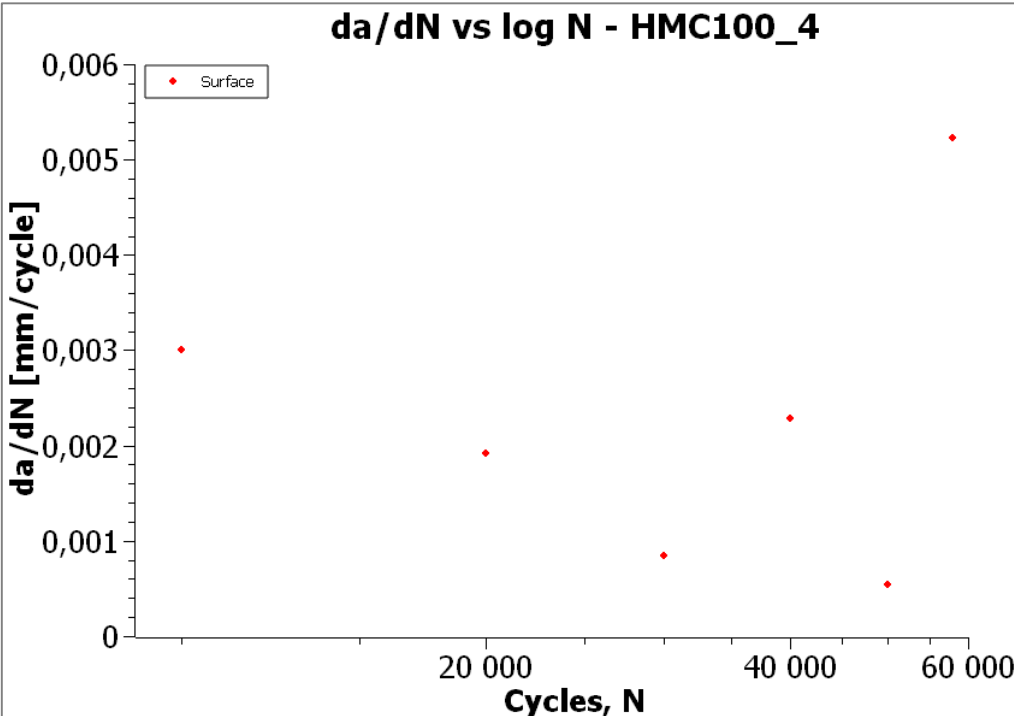
Figure 46: da/dN vs log N for HMC100_4

In figures 47 and 48 the propagation of sample UHMC100_1 is seen. A very high initial growth rate for the surface, compared to the embedded fibre, indicates something wrong in the detection. There is also an offset for the two cracks at 5-10 mm. After initiation, fibres indicate a crack grows at a decent rate up to about 800 cycles where it starts to flatten. The crack propagates slower until about 4 000 cycles where there is a small jump in the embedded measurement.
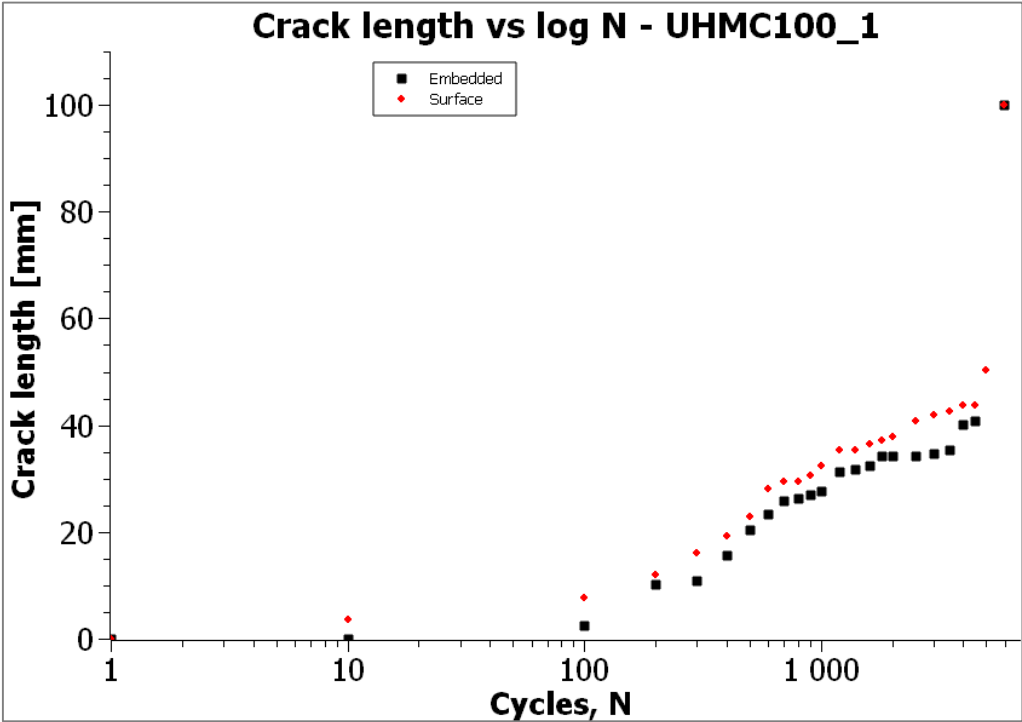
Figure 47: Crack length vs log N for UHMC100_1
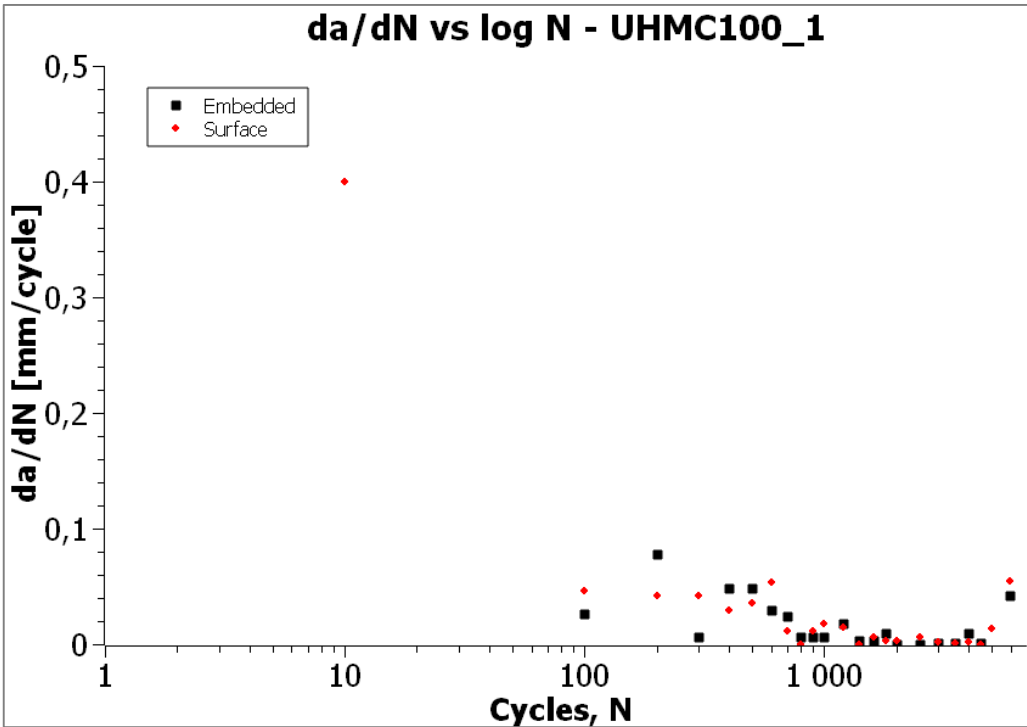
Figure 48: da/dN vs log N for UHMC100_1

UHMC100_2 is shown in figures 49 and 50. The surface fibre is in general showing a crack which is about 5 mm longer for the same given number of cycles as can be seen in figure 49. After initiation, both surface and embedded fibre give a crack growth rate which is on and off, but they both seem to follow the same trend. Overall it seems to be declining until it reaches about 7 000 cycles. At this point the rate picks up a little towards the end.
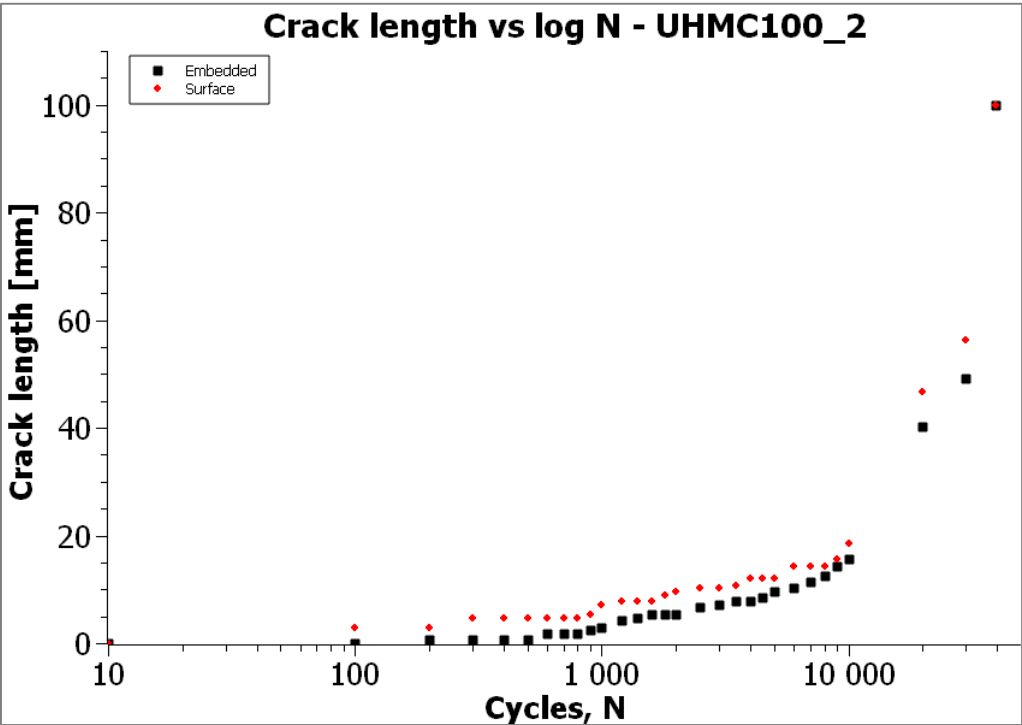
Figure 49: Crack length vs log N for UHMC100_2
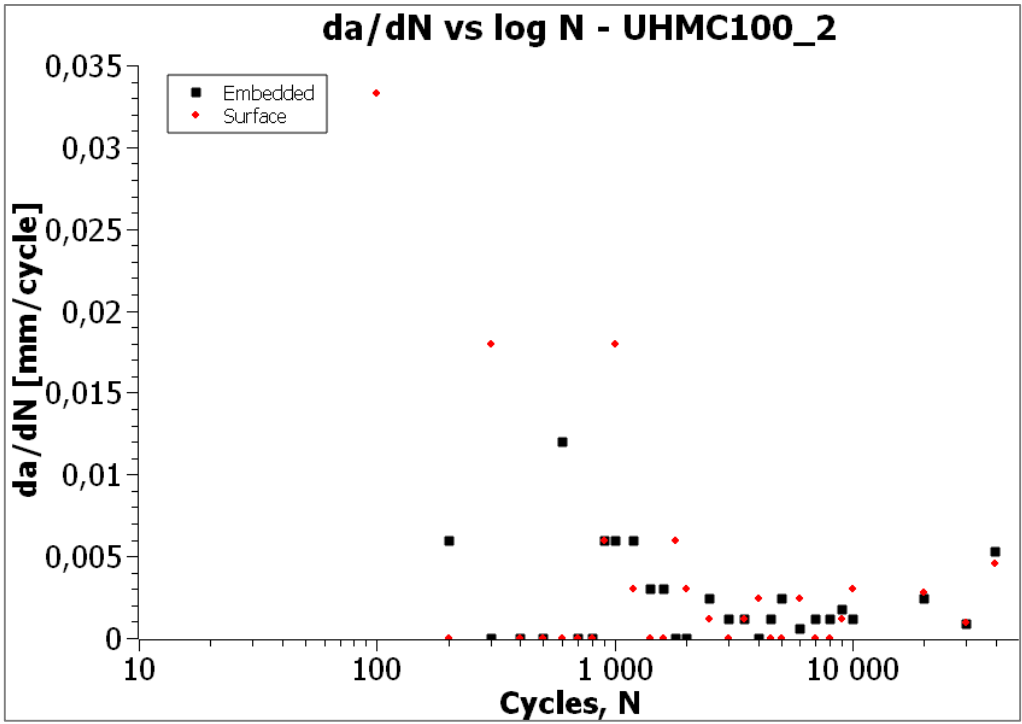
Figure 50: da/dN vs log N for UHMC100_2

UHMC100_3 was only recorded with embedded fibre. After initiation the growth rate declines until about 900 cycles where it is kept fairly steady as seen in figure 52. This can be recognised in the crack length vs cycles plot in figure 51.
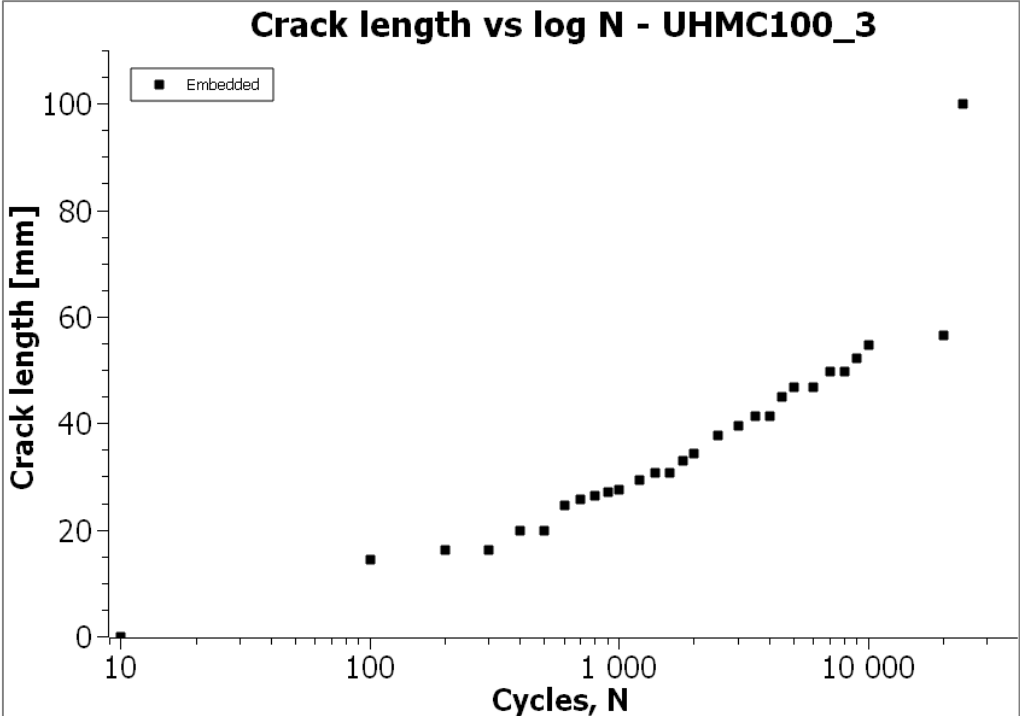
Figure 51: Crack length vs log N for UHMC100_3
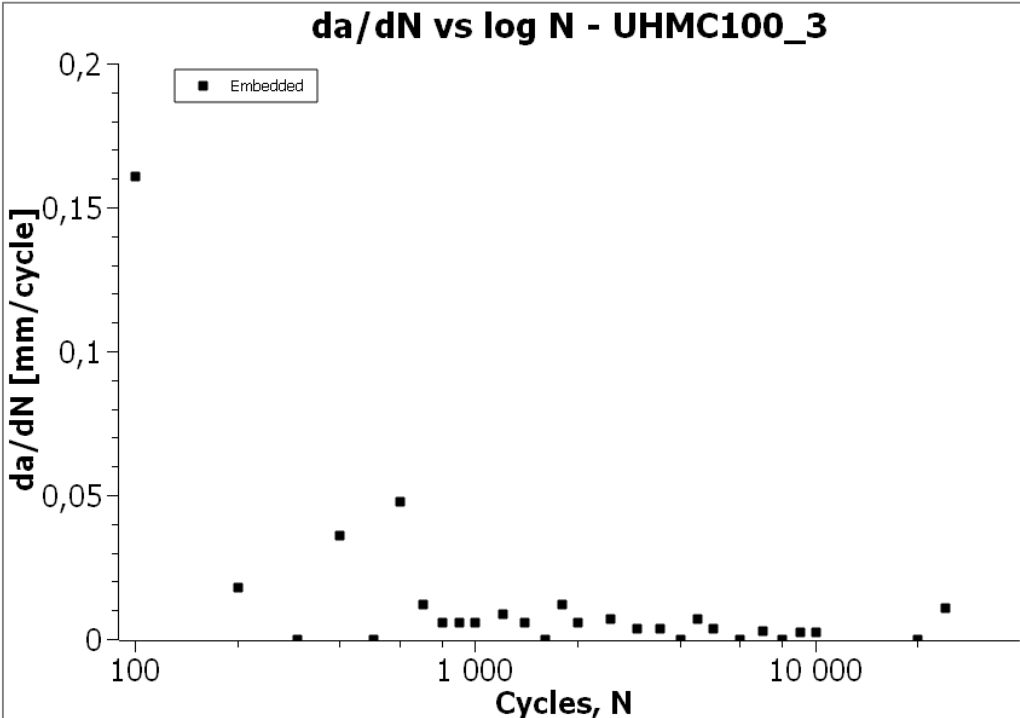
Figure 52: da/dN vs log N for UHMC100_3

In figures 53 and 54 sample UHMC100_4 is shown. Both surface and embedded fibre shows a jump in crack length at 1 000 cycles. When looking at 6 000 and 7 000 cycles in the da/dN plot it can be noticed that what seems like the same jump in crack length appears later for the embedded fibre. A reason can be that the crack tip is not straight, which is discussed in further detail in section 5. The crack length is similar for low number of cycles and deviates about 5-6 mm after 10 000 cycles which could be related to the aforementioned.
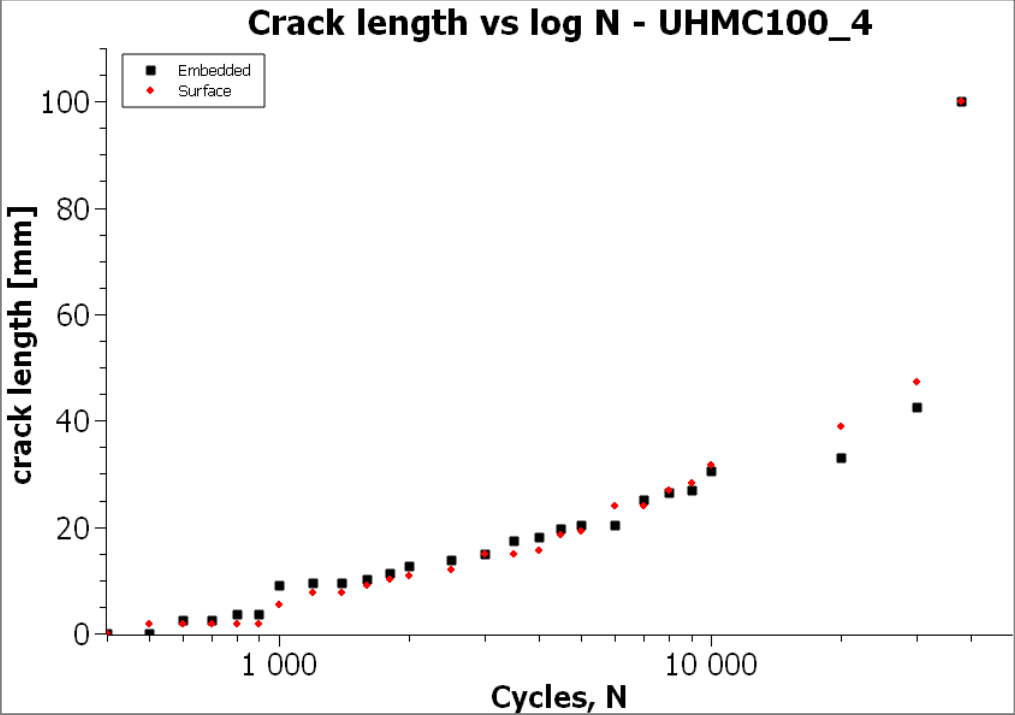
Figure 53: Crack length vs log N for UHMC100_4
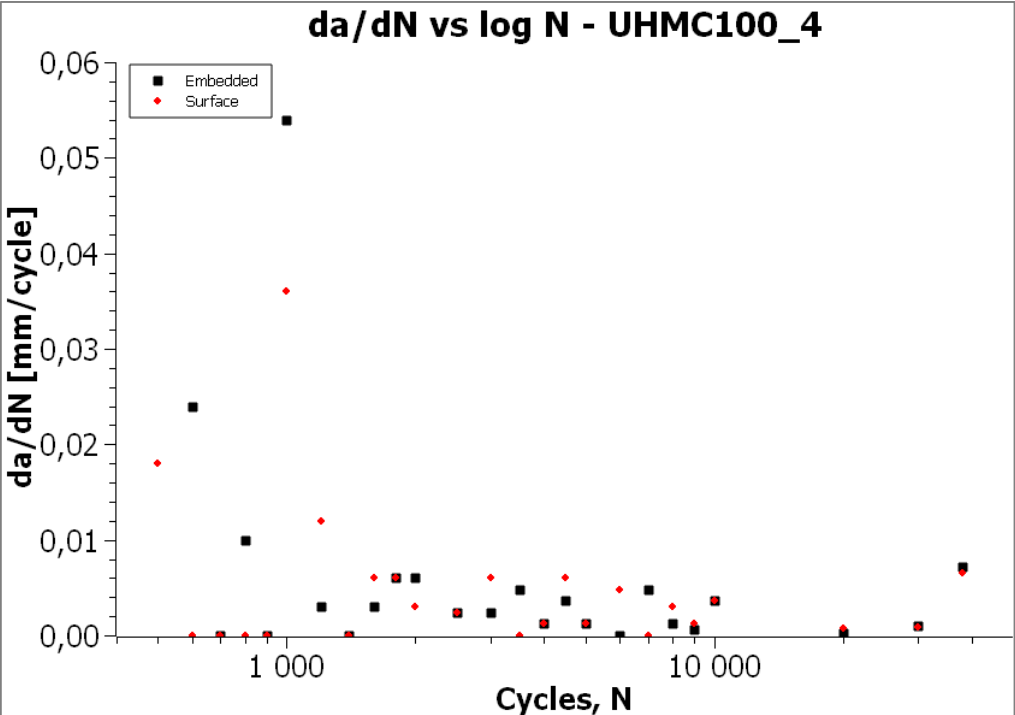
Figure 54: da/dN vs log N for UHMC100_4

4.4 OBR vs strain gauges

The absolute values of the OBR results are less important for this project, however a comparison has been done. The sample HMC100_3 is shown in figures 55, 56 and 57 for 10, 1 000 and 10 000 cycles, respectively.
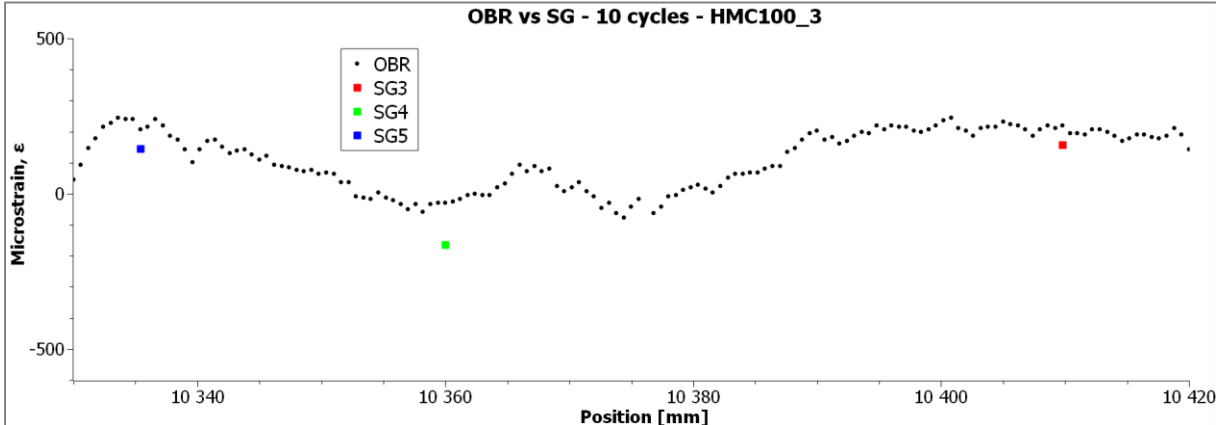
Figure 55: OBR vs SG at 10 cycles for HMC100_3
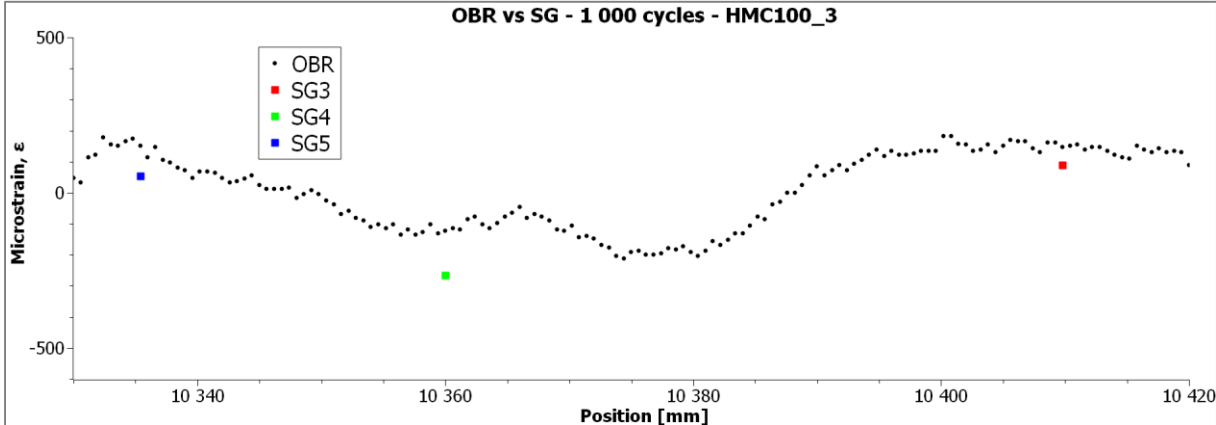
Figure 56: OBR vs SG at 1 000 cycles for HMC100_3
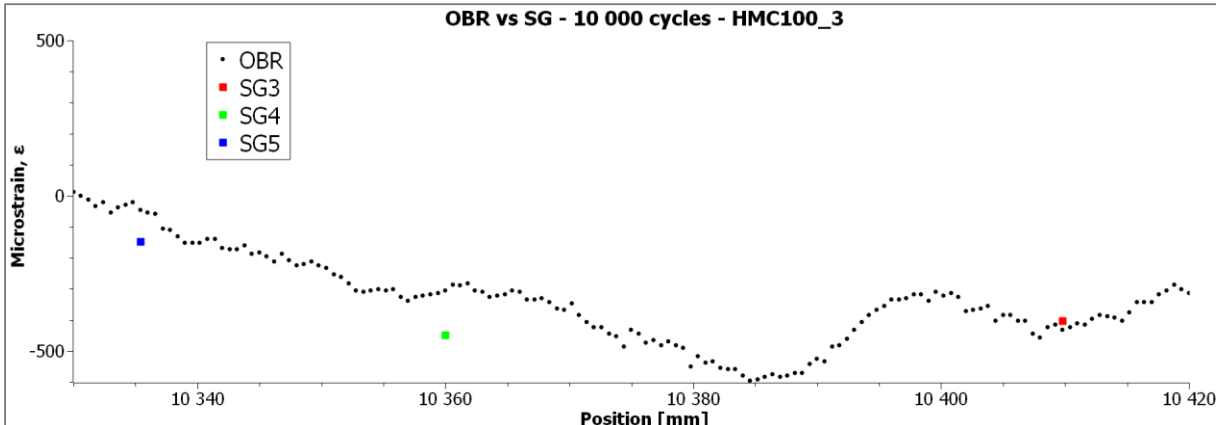
Figure 57: OBR vs SG at 10 000 cycles for HMC100_3

A correlation can be seen between SGs and the fibre but there are some deviations. If the fibre has not been cleaned properly there might be issues getting good results. This can be the

reason for the discrepancy. It should also be noted that since the scale on the y-axis is microstrain, a difference of 50-100, which is a common number, is not a large difference.

The SGs can also be used for detecting crack initiation. It can be seen in figure 11 that SG1 is positioned directly below the overlap end where the crack will first initiate. One example of this is shown in figure 58 with the sample HMC100_3. The initiation is seen as a drop in the strain after around 550 cycles, which is recognized in the graph below, just shy of 600 seconds. This coincides well with the results obtained from the OBR which had initiation in the measurement taken at 600 cycles.
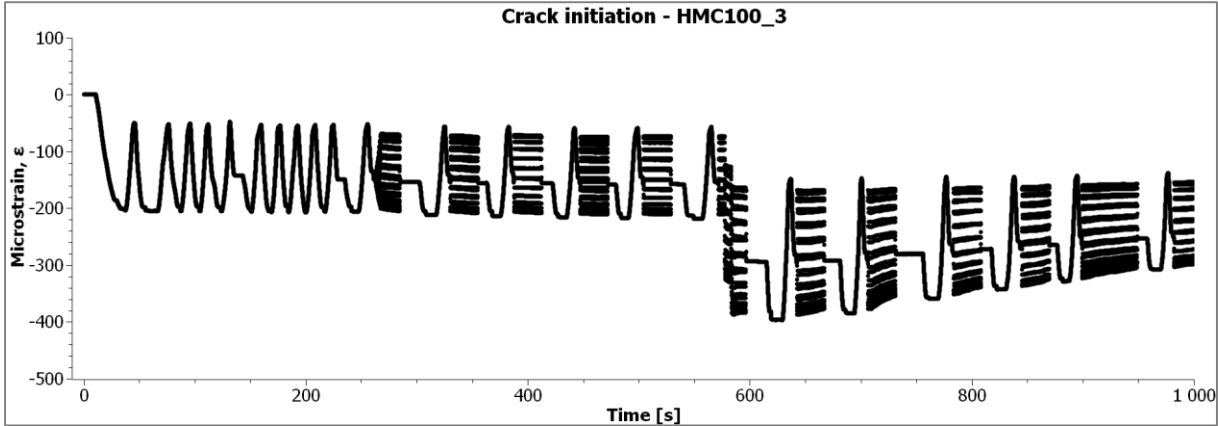
Figure 58 Crack initiation SG in HMC100_3

41

5 Discussion

5.1 Failure

The results in table 6 summarizes the results of the fatigue testing to failure. Of the 100 mm samples all of the tests follow the trend of reduced load giving a longer lifetime, except for the specimen UHMC100_4. As seen in figure 27, there are no signs of adhesive on one side of the fracture surface of the steel. Most of the samples seem to have a very good bond between the adhesive layer and the steel. Adhesive failure could be a reason for the lower than expected fatigue life of this sample. On the other hand, there will be variations in the fatigue life for the same shear stress which could mean that the sample was just in the low end of the spectrum.

It should be noted that a larger number of samples would be preferable in order to get a more representative SN curve. Not only having several samples tested with the same shear stress but also having samples with longer lifespans would be beneficial. The limited number of samples was the reason for not exploring this option.

For the 200 mm specimens there was not performed any static testing to investigate the maximum shear strength before fatigue testing started. There were no clear signs as to why the second sample failed when the load was set to 80% of the first one. More work has to be done in order to see the relationship between different overlap lengths.

5.2 Initiation

There are some issues related to discovering the crack initiation visually. During the early phases of testing there is not much time to thoroughly inspect the specimen for visual cracks. There is little time between each scan, and creep effects, which may occur if the specimen is kept for too long in a loaded state, may give unwanted effects on the experiment. In some cases, though, there is both an apparent visual and audible crack initiation. This was the case for sample HMC100_2, which coincides well with what can be seen in the crack length vs cycles plot and da/dN plots in figures 41 and 42, which display a large initiation crack.

For the embedded fibre, determining the exact location where the crack length is equal to zero is in some cases difficult. At a very low number of cycles, the strain can be low, but when the number of cycles increases the strain increases without any horizontal shift in the peak. In some cases, the peak even grows sharper and appears to grow backwards. An example can be seen in figure 32. The start of the overlap needs to be determined from the graphical data which depends on the resolution of the measurements and in many cases, noise. The lowest resolution for the sensor spacing with the OBR 4600 is 0,6 mm according to Luna [8]. When the crack has started to grow, the spacing seems adequate to give good results, but during initiation of the embedded fibre crack, there might be some points lost. The lower the sensor spacing (and gage length) is, the higher is the resolution and chance of noise problems.

As mentioned in 3.4.2.3, the surface fibre should be easier to determine when it comes to the starting point. However, as seen in samples UHMC100_1 and UHMC100_2 (figures 47 to 50), there are differences when it comes to initiation. Differences in crack length, which seem constant later on, indicate that there might be something wrong initially. As noted previously some samples had audible initiations. As seen in table 7, the UHMC100_2 had a late visual initiation compared to what was detected by fibre, and no sounds were noted early in the

experiment. The large jump seen in figure 50 indicates an abrupt crack growth, which would have been noticed. This seems to indicate that the initiation of this sample by surface fibre has some kind of error. This is also supported by the comparison with embedded fibre which has a lower rate for the initial crack growth. A plausible reason for the difference is that the surface fibre might not have had proper adhesion in the beginning of the overlap, where crack initiates. This could have given the impression of a longer initiation crack.

The initiations were compared with SN curves and can be said to have a good correlation. Especially the visual curve and the surface curve seem similar. Of the results recorded, the specimen UHMC100_2 is the one having the largest discrepancy, as seen in table 10. It can also be seen that the surface fibre in most cases seem to be detecting the initiation earlier than the embedded fibre, for the samples that have both measurements. One reason can be that the embedded fibre is more prone to inaccurate measurements due to noise because the area measured is closer to the end of the fibre.

A note should also be added about the use of SGs in crack initiation. In many cases there were problems importing the text files, which could reach a size of 200 Mb, which is why this method was not utilized to a larger degree. The benefit of using SGs is the possibility of detecting the crack when the machine is running, compared to the OBR which requires a stand still in order to scan. This means that the initiation can be pinpointed in a more exact location. Detection with SGs can also be done during testing by plotting the SG vs time in the data acquisition program and paying attention to the graph while the test is running. This was not considered at the time but should be noted for further testing.

5.3 Crack growth

As seen in figure 23, the crack growth from both sides of the specimen is evident. There should have been put more work into the total crack growth, not only for one side. The problem with the embedded fibre is tracking the crack growth from the composite end as seen on the right side of figure 22. The reason being that the readings within the laminate gives too much noise to effectively being able to track the growth. One reason for this could be that the end of the fibre, which sits within the laminate, might get damaged during testing, which degrades the results.

As mentioned in 3.1 the embedded fibre is laminated in below the composite adherend. For interlaminar cracks it was feared that the embedded fibre may not be able to give proper readings of the crack propagation. By comparing the data from the surface fibres, the results seem to coincide well with only small deviations. This indicates that the crack can still be tracked even though the laminate layer is delaminating further away from the embedded fibre.

When it comes to tracking the crack tip accurately, some difficulties appear. As seen in figure 6 in section 2.2 the strain in the overlap end will increase with increased loading. From figure 32 it can be seen that the same thing appears after an increase in the number of cycles without a shift in x-direction, between cycles 1 and 10. While this image shows a crack initiation, the same thing happens for propagations. The increase in strain indicates that something happens, but there is no shift in the x-direction indicating an increase in crack length. This is most likely a result of the limited resolution in the measurement. This has been the case of for both surface and embedded fibre and is what can be seen as the plateaus in the crack length vs cycles plots.

One explanation for these plateaus can be that the crack front might not be straight [5]. The surface fibre is bonded 9 mm from one edge as shown in figure 16 and the embedded fibre is supposed to be in the centre of the sample. However, in the same figure it can be seen that the optical fibre is not in the centre. The difference in position of the two fibres could be a reason for the different readings if the crack tip propagates at varying rates across the width.

For samples lasting more than 10 000 cycles, the measurements are taken less frequently. This can have an implication on the observed crack growth rate from OBR data. If the second to last and the last measurement, where the latter is at failure, are taken far apart, the average growth over this section can be low. By looking at the propagation to failure of UHMC100_1 in figure 48 the growth rate appears no higher than in the middle region, however the growth in real life will be higher towards the end. It should also be mentioned that for the opposite case, when measurements are taken close together, a high growth rate could be the result. The sample HMC100_2 is an example of the latter where the last two measurements are at 1 400 and 1 424 cycles. The jump in crack length over this short timespan yields a high growth rate in the end, as seen in figure 42. The absolute values of the crack growth rate plots should therefore not be trusted blindly.

In some cases it would be beneficial to have measurements taken at shorter intervals even after 10 000 cycles. One issue is the need to be present when performing scans because the machine has to be paused in order to perform an OBR scan. As indicated in section 3.3.2, the measurement process requires human interaction. This will also mean that for samples run over a longer timespan than in this project, for instance overnight, there would be difficulties logging with OBR.

5.4 Further work

Comparing visual results, optical fibre measurements and strain gauges, has indicated that the measured results found are valid. However, further work would include FE analysis in order to compare initiation with experimental results. In addition, discussions with Giovanni Perillo at Sintef Trondheim highlighted an analysis software working in conjuncture with FEA systems for fatigue analysis. The software is called fe-safe and is made by Dassault Systèmes. This system should be able to estimate fatigue life and highlight critical areas of the design [9].

6 Conclusions

In this thesis 4 specimens were tested under fatigue loading and a total of 8 samples at an overlap length of 100 mm were analysed for crack initiation and crack growth. Extensive knowledge was gained when it comes to preparation and use of optical fibres.

The strain field analysis shows that cracks can be detected with the use of optical fibres. Both optical fibres bonded to the surface of the specimen and embedded fibres yield good results. The accuracy depends on having good measurements with little noise and proper installation of the measuring fibre. Comparison of initiation with strain gauges and visual results provides coinciding results.

Crack propagation has also been investigated with the use of optical fibres. The results show a similar behaviour between cracks detected with surface fibres and embedded fibres.

In addition, an SN curve of the load vs failure has been established on the basis of the experimental work. It has proven that the specimens have a good fatigue behaviour through the gentle slope of the curve. The failures seen through testing are also supported by the relevant theory on this field of study. Mainly the effects of the peel stresses leading to interlaminar failure were reflected in the failure modes of the specimens.

References

[1] Sæter, E., *Fatigue optimization in metal-composite bonds*, 2015

[2] Vassilopoulos, Anastasios P., *Fatigue and Fracture of Adhesively-Bonded Composite Joints*, Elsevier, 2014

[3] Allen, K.W., *Adhesion 15*, Springer Science & Business Media, 2012

[4] Hart-Smith LJ., *Adhesive-bonded Single-lap joints*, NASA CR112236, 1973

[5] Lunder, E.V., *Fatigue of Smart Composite Metal Joints*, 2013

[6] Karatzas V.A., Kotsidis E.A., Tsouvalis N.G., *Bond Strength Tests*, 2012

[7] Campilho, R.D.S.G., *Natural Fibre* Composites, CRC Press, 2015

[8] Luna Technologies, 2014, revision 004. *Data Sheet*. [pdf]. Available at: http://lunainc.com/wp-content/uploads/2014/05/OBR4600_Data-Sheet_Rev-05.pdf [Accessed June 09 2016].

[9] Dassault Systems, 2014. *fe-safe Datasheet*. [pdf]. Available at: http://www.3ds.com/fileadmin/PRODUCTS-SERVICES/SIMULIA/RESOURCES/simulia-fe-safe-datasheet.pdf [Accessed June 10 2016]

Appendix

A.1 Specimen raw data

Specimen	Length [mm]		Width [mm]					Thickness overlap [mm]				
HMC 100_1	98,8	99,1	25	25	25,1	25,1	25,1	12,8	13,2	13,5	13,5	13,6
HMC 100_2	98,7	99	25	25	25	25	25	12,5	13,4	13,6	13,6	13,6
HMC 100_3	98,4	98,4	24,5	24,5	24,5	24,4	24,4	12,8	13,4	13,6	13,6	13,4
HMC100_4	98,9	97,4	24,5	24	23,6	23,3	21,5	12,6	13,4	13,5	13,5	13,5
UHMC 100_1	99,3	99,5	25,3	25,3	25,3	25,2	25,3	12,2	12,9	13,2	13	12,8
UHMC 100_2	99,4	99,1	23,7	23,7	23,7	23,7	23,7	12	12,9	13	13	12,8
UHMC 100_3	99,1	99,1	30	30,1	30,1	29,9	29,9	11,9	12,9	13,2	13,1	12,9
UHMC100_4	98,7	99,4	24,9	25	24,9	24,9	25	12,2	12,8	13,1	13,1	12,9
HMC200_5	199,8	199,9	26	25,8	25,3	25,2	25	12,7	13	13,1	13	12,9
UHMC200_1	200,2	200,8	25,1	24,9	25	25	25	12,4	12,8	12,7	12,7	12,7

Table 11 Raw data specimen measurements

A.2 Plots for crack length vs number of cycles and da/dN vs number of cycles
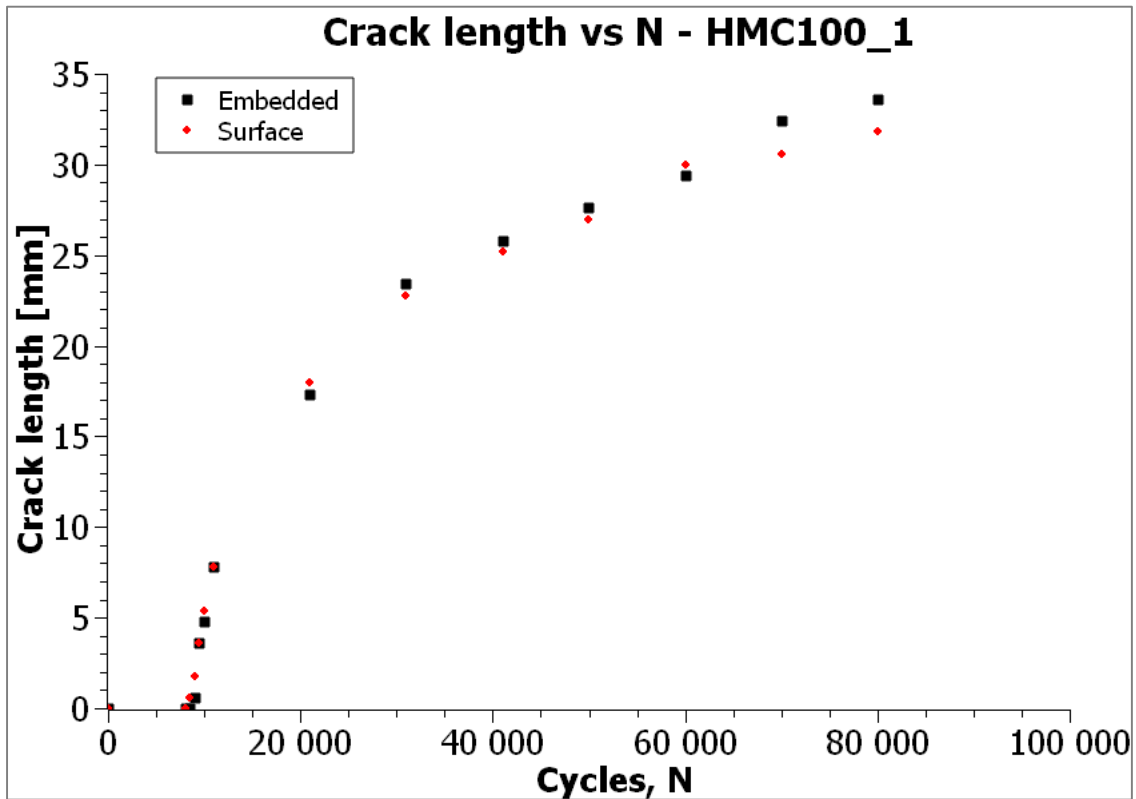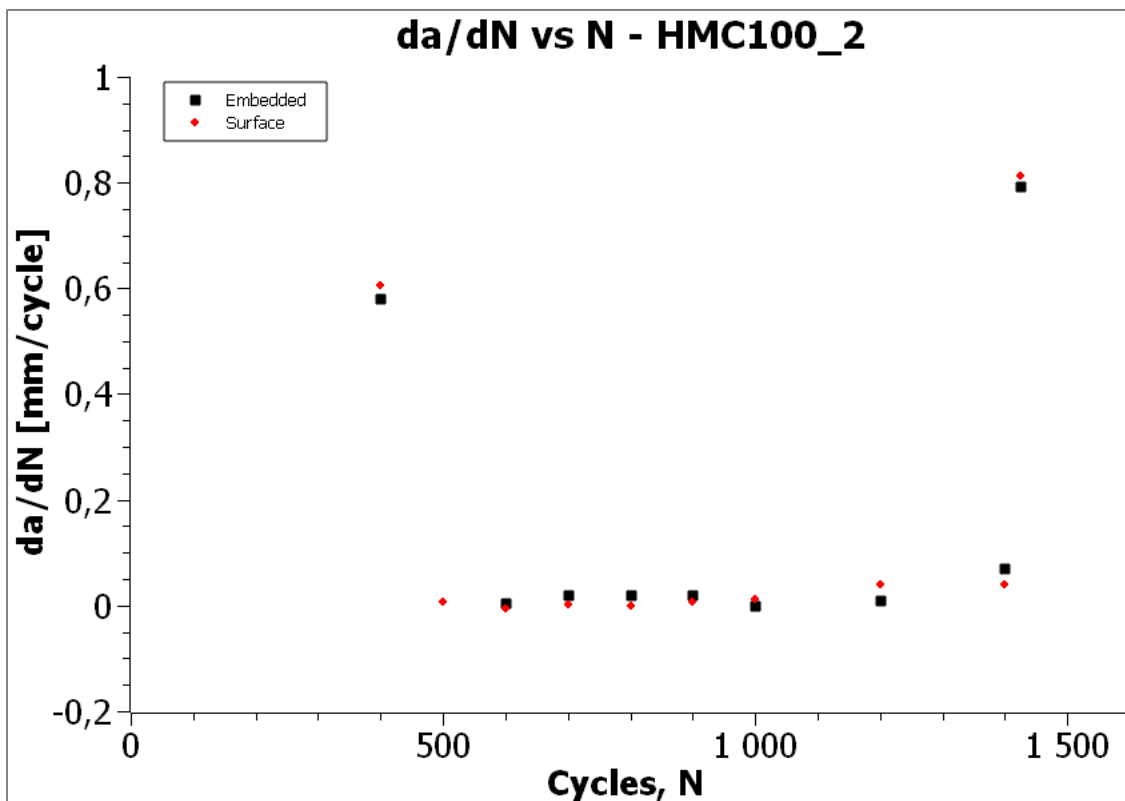

Figure 59: Crack length vs N for HMC100_1
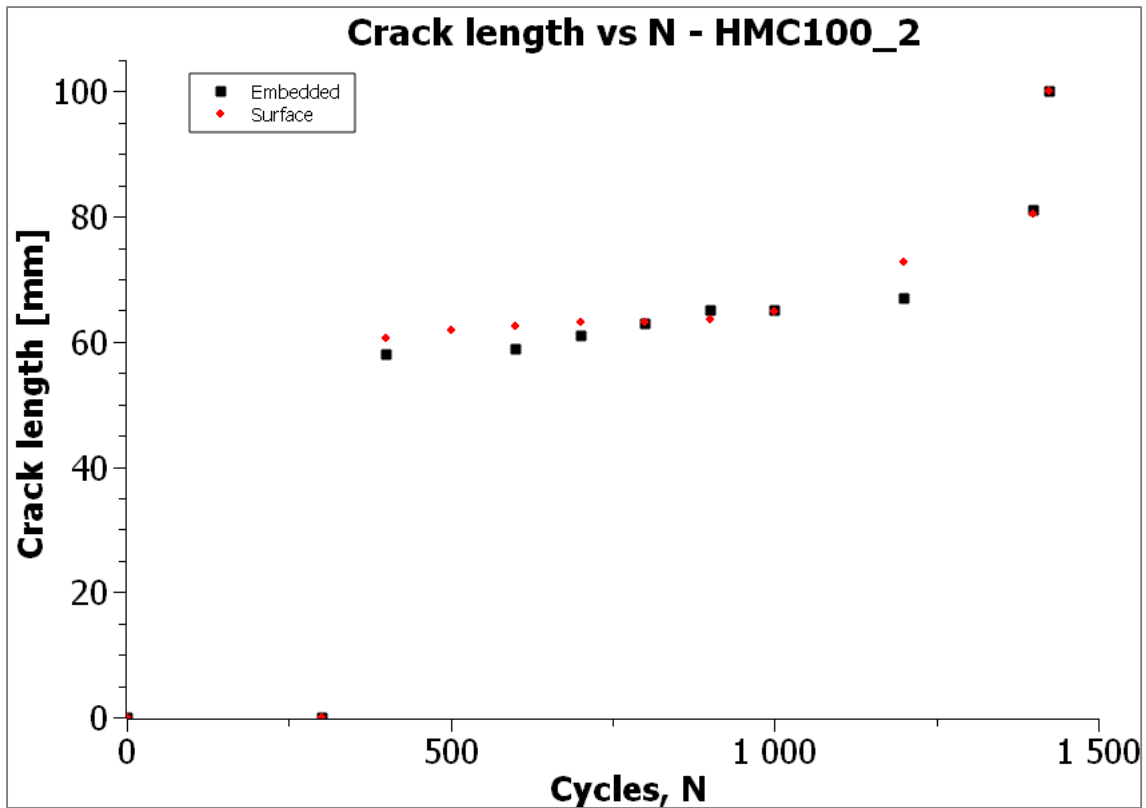

Figure 60: da/dN vs N for HMC100_1

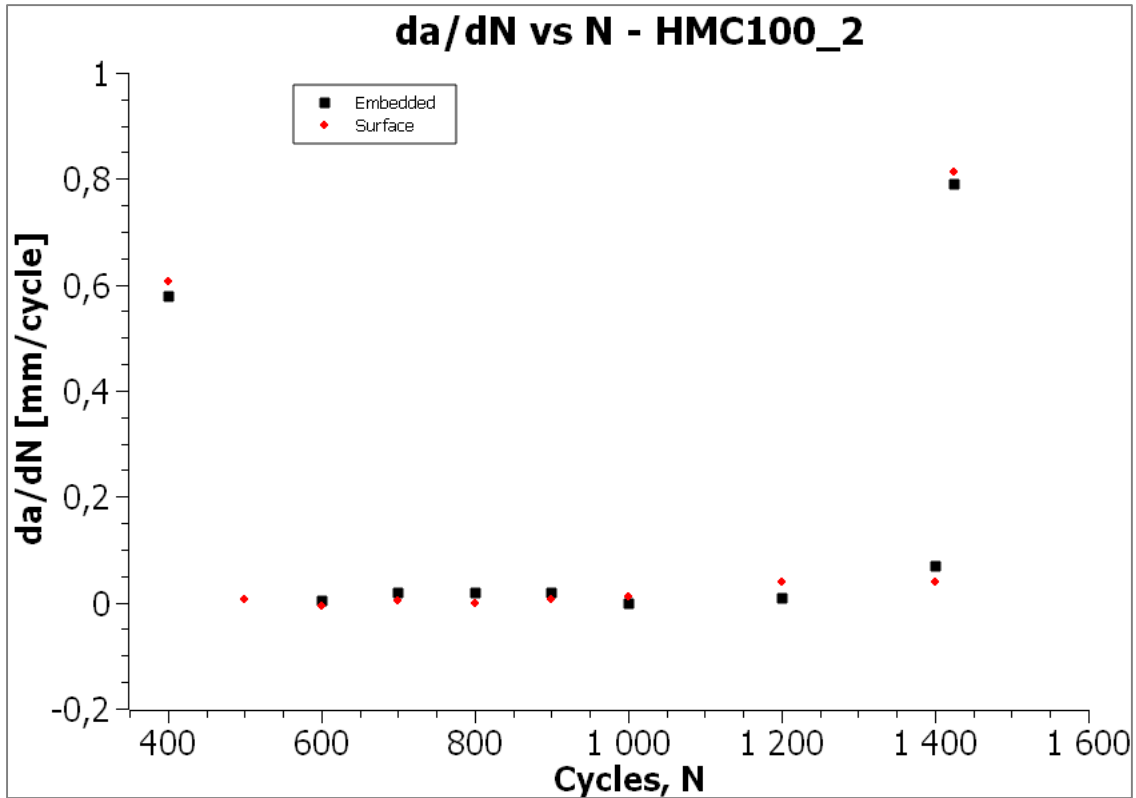*Figure 61: Crack length vs N for HMC100_2*

Figure 62: da/dN vs N for HMC100_2

Figure 63: Crack length vs N for HMC100_2

Figure 64: da/dN vs N for HMC100_3

Figure 65: Crack length vs N for HMC100_4

Figure 66: da/dN vs N for HMC100_4

Figure 67: Crack length vs N for UHMC100_1

Figure 68: da/dN vs N for UHMC100_1
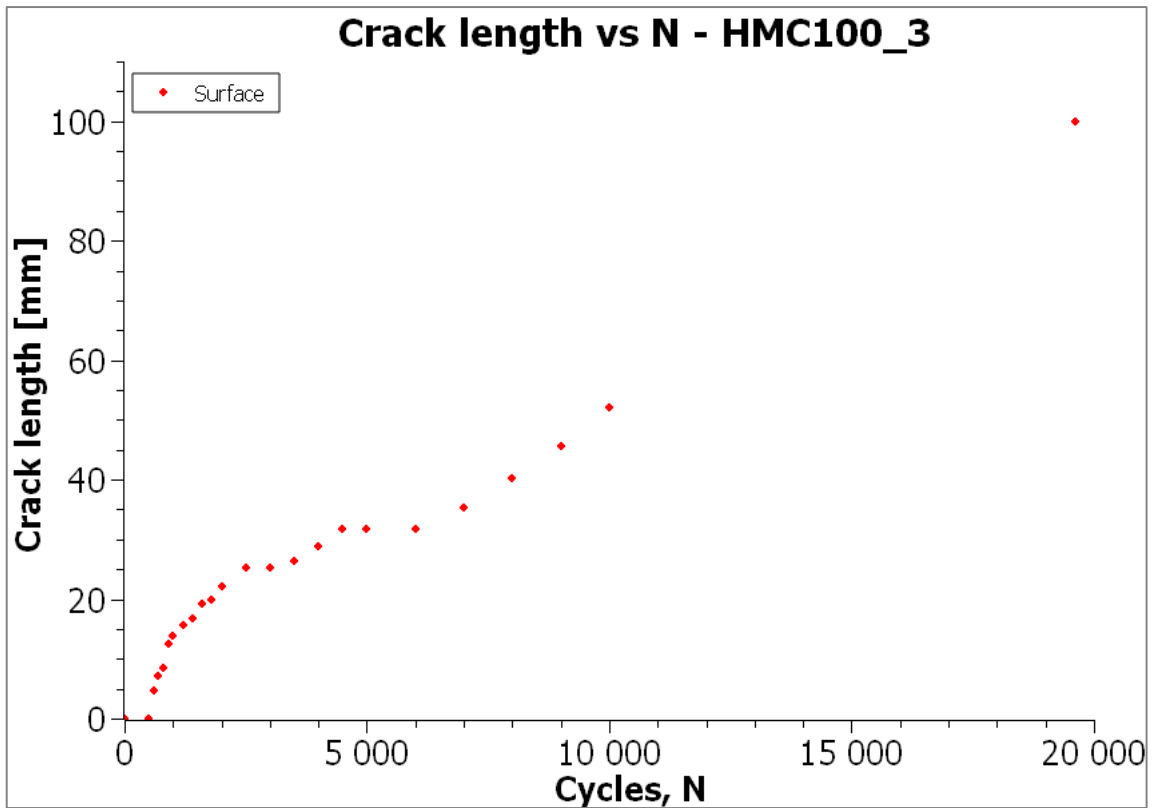
Figure 69: Crack length vs N for UHMC100_2

Figure 70: da/dN vs N for UHMC100_2

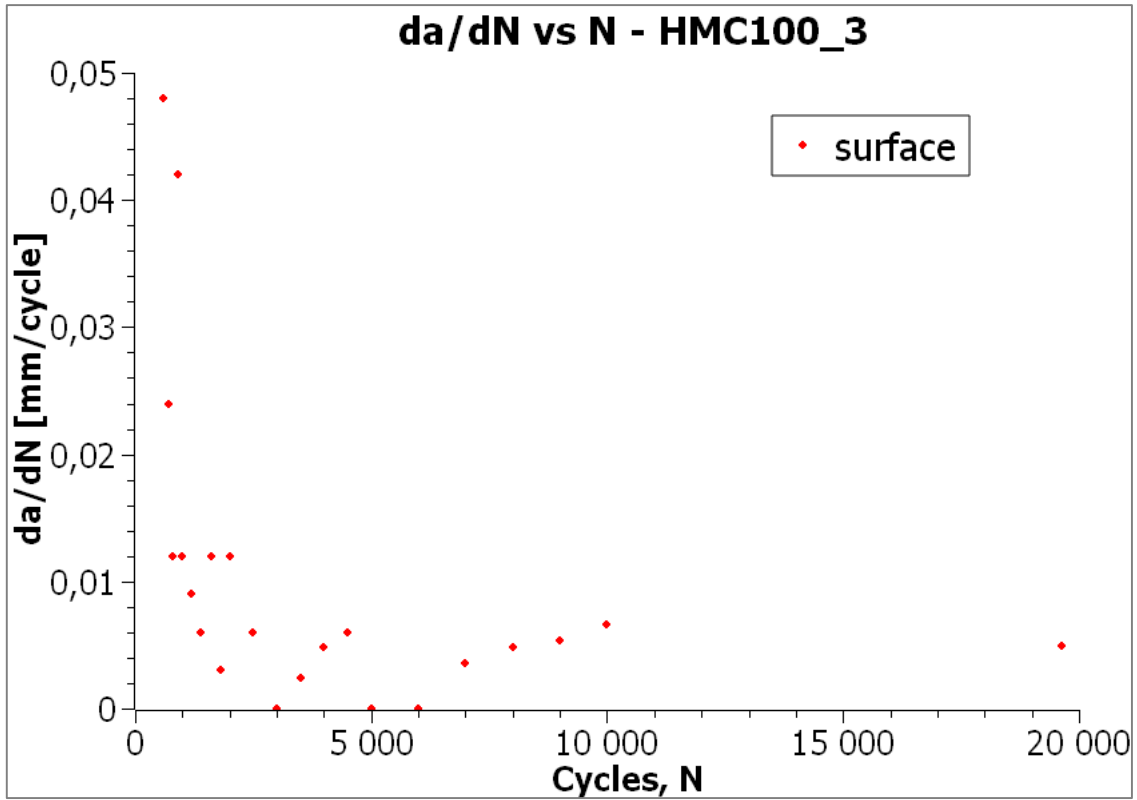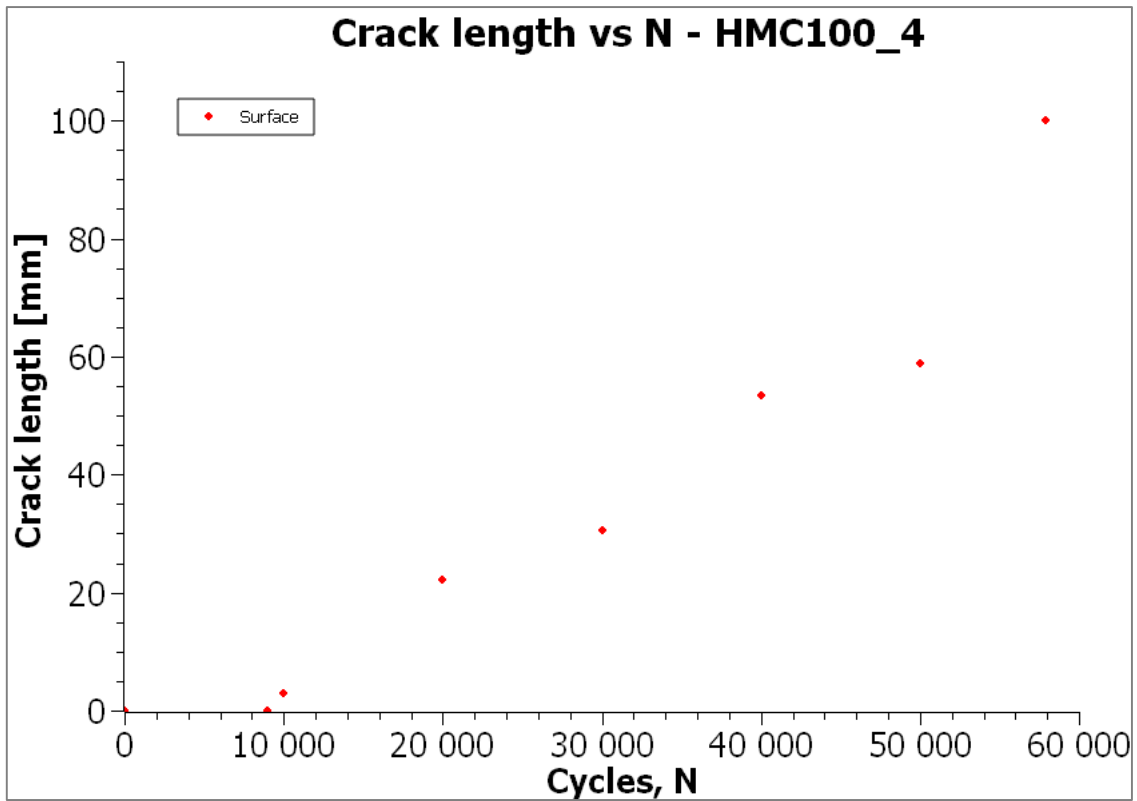*Figure 71: Crack length vs N for UHMC100_3*
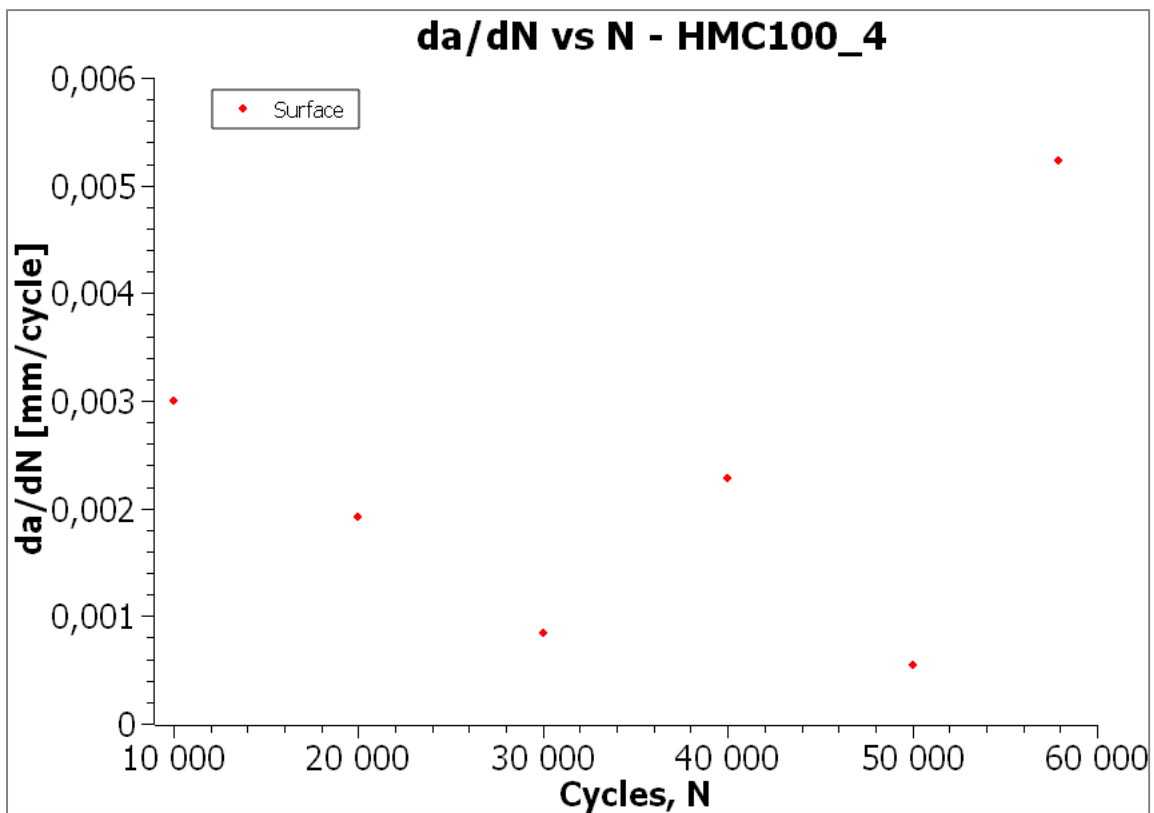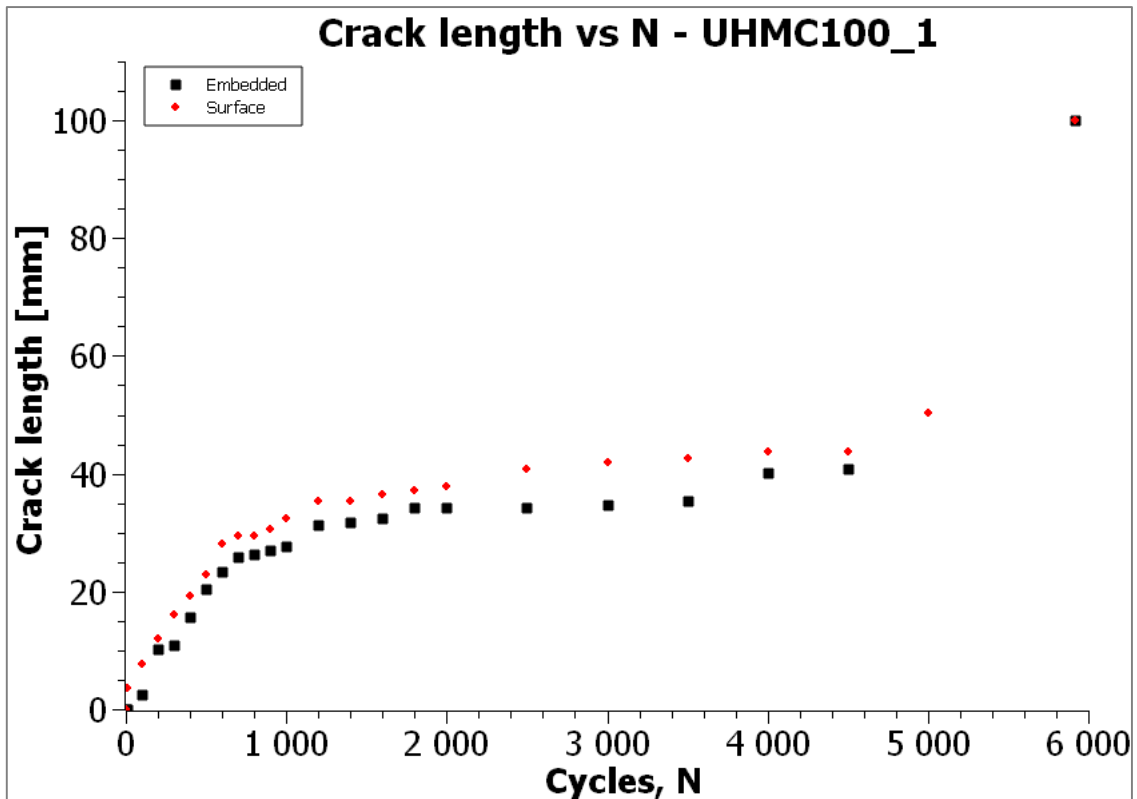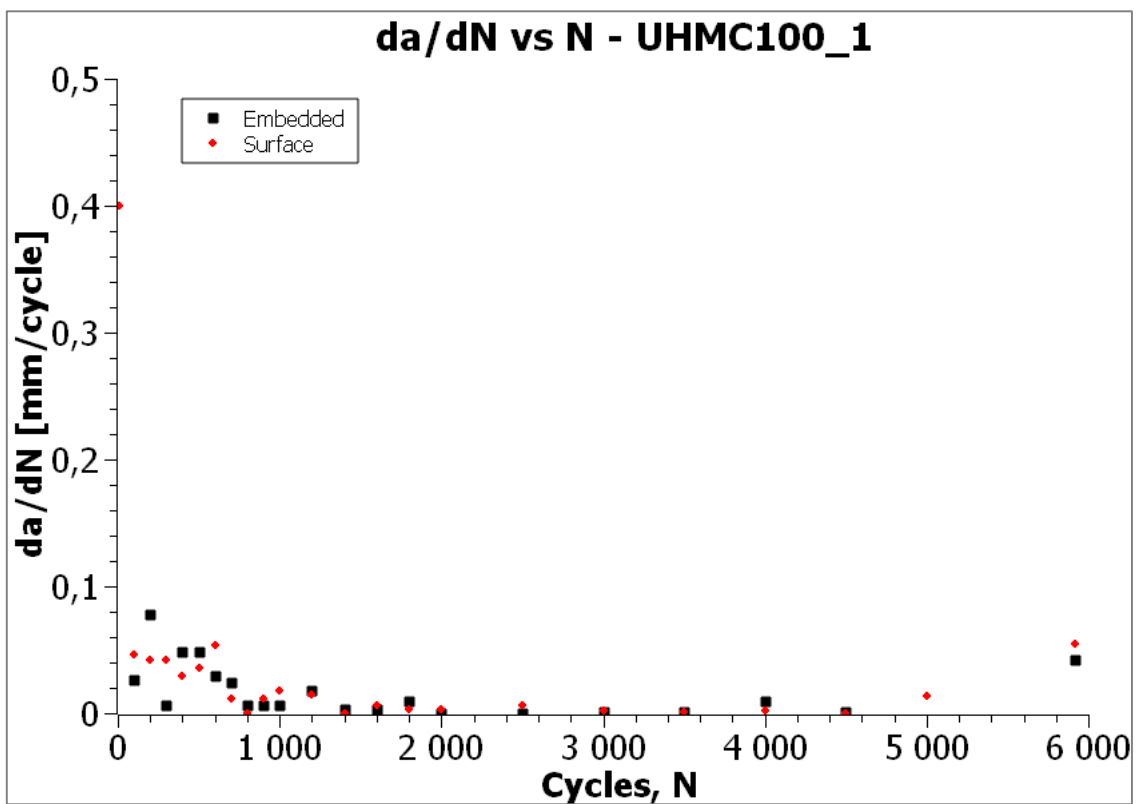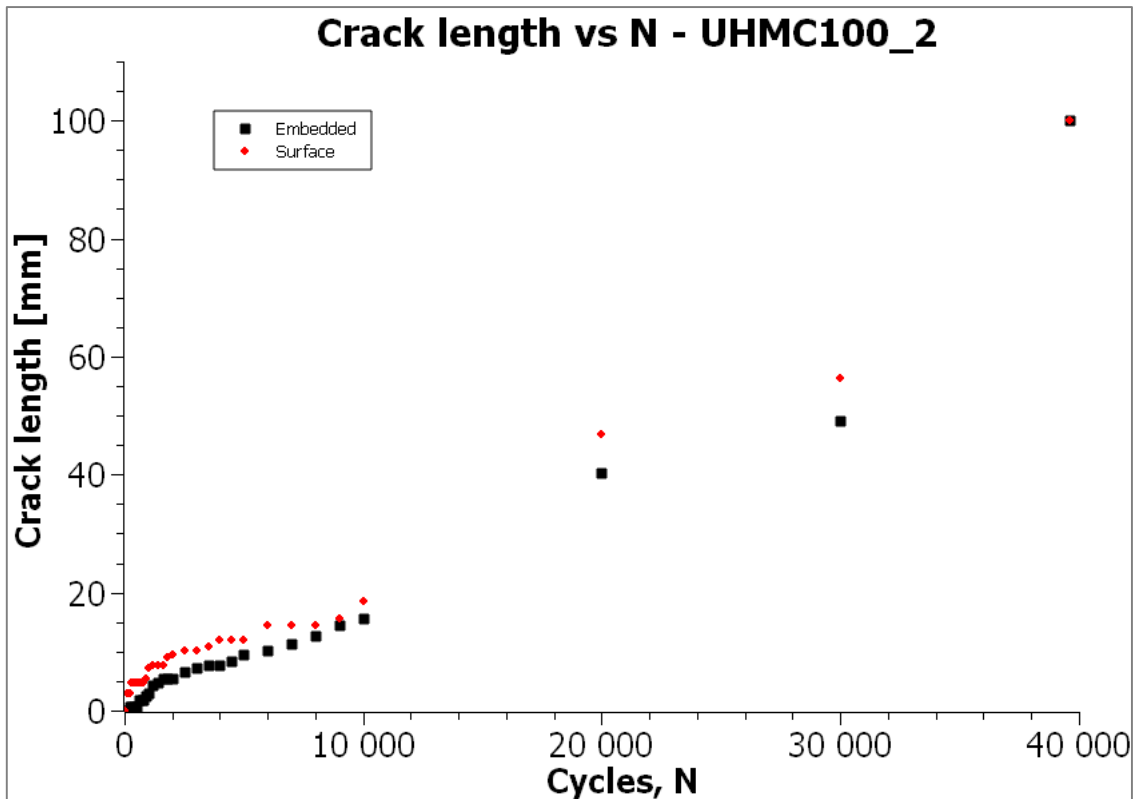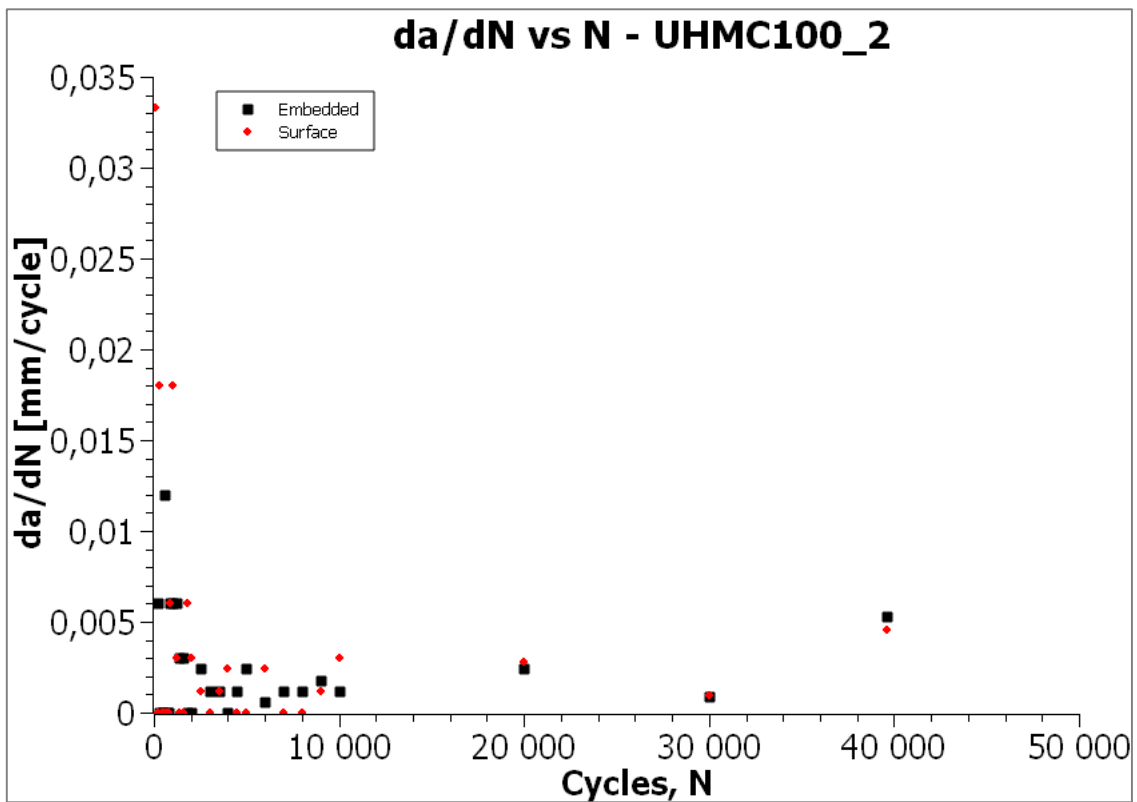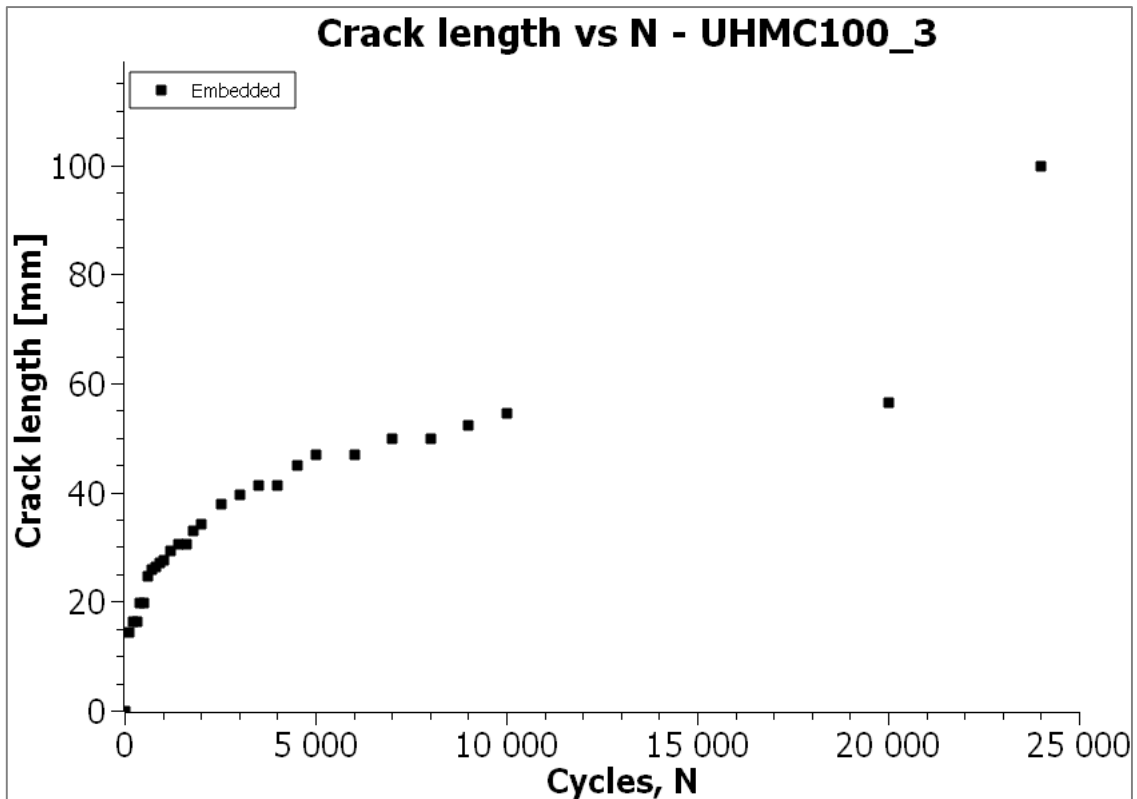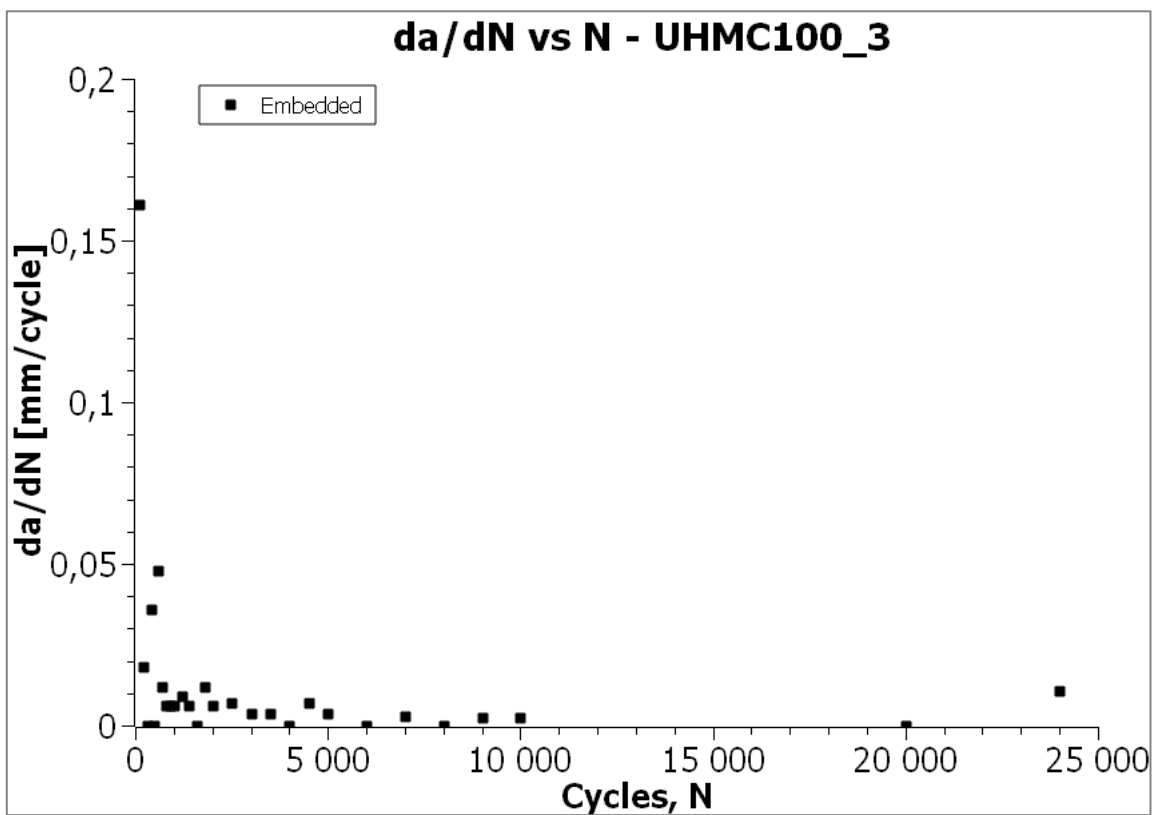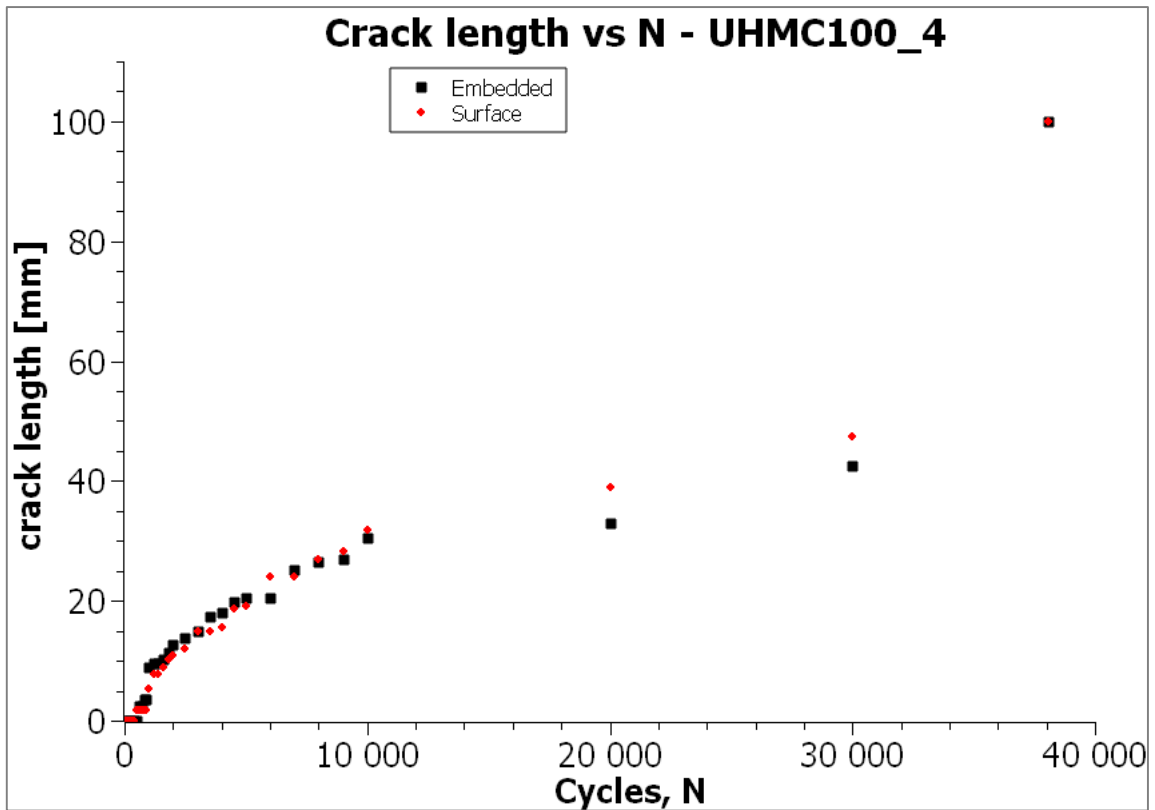

Figure 72: da/dN vs N for UHMC100_3

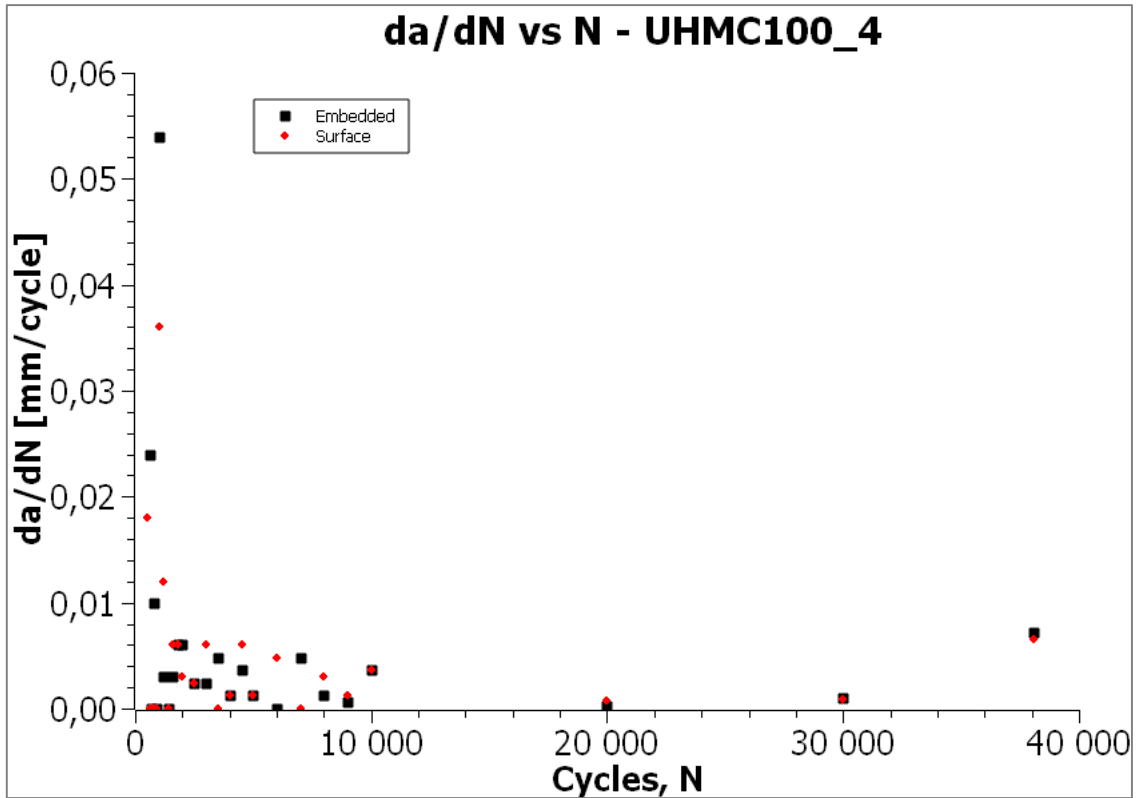*Figure 73: Crack length vs N for UHMC100_4*

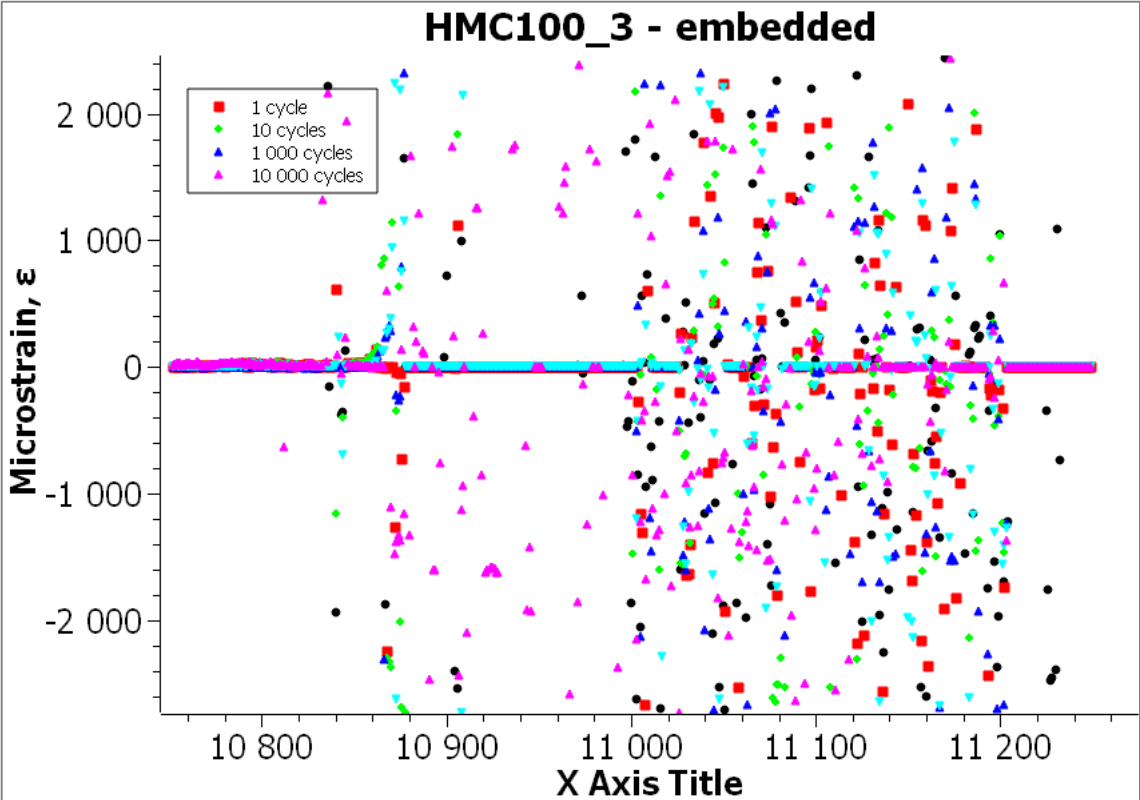*Figure 74: da/dN vs N for UHMC100_4*

A.3 OBR plot

Figure 75: Noise in HMC100_3

A.4 Risk Assessment

Sikkerhets- og kvalitetsgjennomgang av laboratorietester og verkstedsarbeid
Safety and Quality Evaluation of Activities in the Laboratory and Workshop

NTNU

Perleporten

1 Identifikasjon – *Identification*		Dokumentnr. – *Document no.*:		
Kundenavn – *Customer name*		Prosjektnavn – *Project name*		Projektnr. – *Project no.*
Erik Jøeten (E.J.)		Fatigue resistance of adhesive joints		
Beskrivelse av arbeid – *Description of job*				Dato – *Date*
Cutting samples with band saw and fatigue testing				05.02.16

2 Projekt – *Team*			
Prosjektleder og organisasjon – *Project manager and organisation*	E.J.	Ansvarlig for instrumentering – *Responsible for instrumentation.*	E.J.
Leiestedsansvarlig – *Laboratory responsible*	E.J.	Operatør – *Operator*	E.J.
Auditør for sikkerhets og kvalitetsgjennomgang – *Auditor for safety check*	E.J.	Ansvarlig for styring av forsøk – *Responsible for running the experiment.*	E.J.
Ansvarlig for eksperimentelt faglig innhold – *Responsible for experimental and scientific content*	E.J.	Ansvarlig for logging av forsøksdata – *Responsible for logging and storing experimental data*	E.J.
Ansvarlig for dimensjonering av last og trykkpåkjente komponenter – *Responsible for dimensioning load bearing and pressurized components*	E.J.	Ansvarlig for montering av testrigg – *Responsible for building the rig*	E.J.

3 Viktig!! – *Important!!*		I: Ja – *Yes* / N: Nei - *No*
Er arbeidsordren signert? – *Is the work order signed?*		Y
Har operatøren nødvendig kurs/trening i bruk av utstyret? – *Has the operator the required courses/training on the equipment?*		Y
Har operatøren sikkerhetskurs? (påbudt) – *Has the operator followed the safety courses? (mandatory)*		Y
Kan jobben gjøres alene? - *Can the work be done alone?*		Y
- Dersom ja, er det med visse forbehold (for eksempel, må bruke alarm, ha avtale med noen som kommer innom med jevne mellomrom eller lignende). Dette må vurderes i Seksjon 5. *If yes, the work may have to be done under special conditions (e.g. must use the alarm, have agreement with somebody coming back periodically or similar). This shall be evaluated in Section 5.*		N

4.1 Sikkerhet – *Safety* (Testen medfører – *The test contains*)				I: Ja – *Yes* / N: Nei - *No*
Stor last – *Big loads*	N	Brannfare – *Danger of fire*		N
Tunge løft – *Heavy lifting*	N	Arbeid i høyden – *Working at heights*		N
Hengende last – *Hanging load*	N	Hydraulisk trykk – *Hydraulic pressure*		Y
Gasstrykk – *Gas pressure*	N	Vanntrykk – *Water pressure*		N
Høy temperatur – *High temperature*	N	Lav temperatur – *Low temperature*		N
Deler i høy hastighet – *Parts at high velocity*	N	Farlige kjemikalier – *Dangerous chemicals*		N
Sprutakselerasjon ved brudd – *Sudden acceleration at fracture/failure*	Y	Forspente komponenter – *Pre-tensioned components*		N
Farlig støv – *Dangerous dust*	Y	Kraftig støy – *Severe noise*		N
Klemfare – *Danger of pinching*	N	Roterende deler – *Rotating parts*		N

4.2 Påkrevet verneutstyr – *Required safety equipment*				I: Ja – *Yes* / N: Nei - *No*
Briller (påbudt) – *Glasses (mandatory)*	Y	Vernesko – *Safety shoes*		N
Hjelm – *Helmet*	N	Hansker – *Gloves*		N
Skjerm – *Screen*	N	Visir – *Visir*		N
Hørselsvern – *Ear protection*	N	Løfteredskap – *Lifting equipment*		N
Yrkessele, fallsele, etc. – *Harness ropes, other measures to prevent falling down.*	N			

Rev. 09 – Nov 2013

Page 1 of 7

57

Sikkerhets- og kvalitetsgjennomgang av laboratorietester og verkstedsarbeid

NTNU
Pemloporten

5.1 Beskrivelse av aktivitet – *Description of the activity (see Appendix)*

Vurdering skal være basert på en skriftlig prosedyre for bruk av maskinen. I enkelte tilfeller kan prosedyre bli beskrevet direkte i tabellen nedenfor.

The evaluation shall be based on a written operating procedure for the machine. For simple cases the procedure can be directly described in the tables below.

Nr.	Beskrivelse av aktivitet – Description of activity	Fare – Danger	Lov, forskrift m.l. – Legal requirements	Prosedyre nr. – Procedure no.	Sannsynlighet – Probability	Konsekvens – Consequence	Risiko – Risk
1	Cutting with band saw	Cut finger	NTNU HMS			D	1 D
2		Towards free cutting	NTNU HMS		3	D	3 D
3		Cutting dust	NT DU HMS		2	A	2 A
4	Fatigue testing	Splinters from fretture	NTNU HMS		1	D	1 D

5.2 Korrigerende Tiltak – *Corrective Actions*

Nr.	Korrigerende tiltak – Corrective action	Sannsynlighet- – Probability	Konsekvens – Consequence	Risiko – Risk	Utført dato – Date of action
1	Get protection plate	C	D	1 D	05.01.16
2	Use glasses	3	A	3 A	"
4	Use protective screen	1	A	1 A	"

58

Sikkerhets og kvalitetsgjennomgang av laboratorietester og verkstedsarbeid

⊡ NTNU
Perleporten

5.3 Fellkilder – *Reasons for mistakes/errors*
Sjekkliste: Er følgende fellkilder vurdert? – Check list: Is the following considered?   J: Ja – Yes / N: Nei – No

Tap av strøm – *Loss of electricity*	Y	Overspenning – *Voltage surge*	Y
Elektromagnetisk støy – *Electromagnetic noise*	Y	Manglende aggregatkapasitet av hydraulikk – *Insufficient power of the machine*	Y
Jordfeil – *Electrical earth failure*	Y	Vannsprut – *Water jet*	Y
Ustabilt trykk av hydraulikk/kraft – *Unstable pressure or hydraulic force*	Y	Tilfeldig avbrudd av hydraulikk/kraft – *Unintended interruption of power supply*	Y
Last-/ forskyvnings grenser etablert ? – *Are load and displacement limits established?*	Y	Lekkasjer (slanger/koblinger, etc.) – *Leakage of pipes, hoses, joints, etc.*	Y
Mulige påvirkninger fra andre aktiviteter – *Possible interference from other activities*	Y	Mulige påvirkninger på andre aktiviteter – *Possible interference towards other activities*	Y
Problemer med datalogging og lagring – *Troubles in loading and storage*	Y	Brann i laboratoriet – *Fire in the laboratory*	Y

6 Kalibreringsstatus for utstyr – *Calibration of equipment*
(ex: load cell, extensometer, pressure transducer, etc)

I.D.	Utstyr - *Equipment*	Gyldig til (dato) – *Valid until (date)*

7 Sporbarhet – *Traceability*
Eksisterer – Is there   J: Ja – Yes / N: Nei – No

Er alle prøvematerialene kjente og identifiserbare? – *Are all experimental materials known and traceable?*	Y
Eksisterer det en plan for marketing av alle prøvene? – *Is there a plan for marking all specimens?*	V
Er dataloggingsutstyret identifisert? – *Is the data acquisition equipment identified?*	Y
Er originaldata lagret uten modifikasjon? – *Are the original data stored safely without modification?*	Y
Eksisterer det en backup-prosedyre? – *Is there a back-up procedure for the data (hard disk crash)?*	Y
Eksisterer det en plan for lagring av prøvestykker etter testing? – *Is there a plan for storing samples after testing?*	Y
Eksisterer en plan for avhending av gamle prøvestykker? – *Is there a plan for disposing of old samples?*	Y

8 Kommentarer – *Comments*

9 Signaturer – *Signatures*
Godkjent (dato/sign) – Approved (date/signature)

Prosjektleder – *Project leader*	Verifikatør – *Verifier*	Godkjent – *Approved by*